1993ApJ...416..425M

THE ASTROPHYSICAL JOURNAL, 416:425–443, 1993 October 20
© 1993. The American Astronomical Society. All rights reserved. Printed in U.S.A.

EARLY-TYPE GALAXIES, DARK HALOS, AND GRAVITATIONAL LENSING STATISTICS

DAN MAOZ AND HANS-WALTER RIX[1]
Institute for Advanced Study, Princeton, NJ 08540
Received 1992 December 28; accepted 1993 April 27

ABSTRACT

We present calculations of the expected statistics of gravitational lensing of quasars in the *Hubble Space Telescope* snapshot survey. We first model early-type (elliptical and S0) galaxies using their observed surface brightness profiles and dynamically inferred mass-to-light ratios. Our work improves upon previous calculations, which have generally approximated the galaxy potentials by isothermal spheres. For standard cosmologies, the predicted number of lensed quasars in the survey is 1.1–2.8, 98% of which have image separations less than 2″, compared to the four lenses observed, two of which have separations greater than 2″. These constant mass-to-light ratio models are rejected. Even in an extreme model in which every early-type galaxy is assumed to reside in a dense cluster, the probability of producing lenses with greater than 2″ separation is too small. Clusters are inefficient in enlarging the image separations because too much fine tuning between the cluster mass profile and the galaxy position within the cluster is required. The predicted number of lenses and their image separations agree well with the observations (at the $\sim 30\%$ level) if a dark isothermal halo component is added to the early-type galaxies. The halo component must have a core radius small enough to yield an effectively flat rotation curve and a velocity dispersion $\sigma^* \gtrsim 270$ km s^{-1} for and L^* galaxy. The observed lensing statistics strongly favor the hypothesis that dark halos are generically present in early-type galaxies. Although stars dominate the mass at small radii and determine the lensing cross section, the dark matter at larger radii increases the typical image separation and enhances the lensing probability through the magnification bias. Models with a cosmological constant λ produce more lens systems, but with similar image separations to standard models. Models with nonzero λ therefore overpredict the number of small-separation lenses if there are no dark halos or overpredict the total number of lenses if a halo component is included. The observations constrain λ to be $\lesssim 0.7$, so that a cosmological constant no longer provides an attractive solution for the "age problem" of the universe. These conclusions are robust with respect to uncertainties in the model parameters.

Subject headings: dark matter — galaxies: structure — gravitational lensing — quasars: general

1. INTRODUCTION

The statistics of gravitational lensing can provide a powerful probe of the geometry and the mass content of the universe out to large redshifts (e.g., Refsdal 1964; Press & Gunn 1973; Blandford & Narayan 1992). Turner, Ostriker, & Gott (1984, hereafter TOG) calculated lensing probabilities and image separation distributions under the assumption that the lensing galaxies can be modeled as an unevolving population of singular isothermal spheres (SIS) characterized by their one-dimensional velocity dispersions, σ. Hinshaw & Krauss (1987) and Krauss & White (1992) studied the effects of removing the central singularity by means of a core. Blandford & Kochanek (1987), Kochanek & Blandford (1987), and Kochanek (1991b) investigated the effect of lens ellipticities and observational selection effects on lensing cross sections and image configurations. Gott, Park, & Lee (1989), Turner (1990), Fukugita & Turner (1991, hereafter F&T), and Kochanek (1992, 1993) studied lensing in arbitrary Robertson-Walker cosmologies. Turner (1980) and F&T also emphasized the effects of magnification bias, the over-representation of lensed quasars in a bright sample due to amplification by lensing of fainter quasars to that brightness. The effect of galaxy evolution on lensing probabilities has been studied by Mao (1991) and that of combining a non-zero core radius and an elliptical potential has been studied by Wallington & Narayan (1993).

Nearly all of the above studies have concentrated on the isothermal potential, i.e., a mass density distribution proportional to r^{-2} in radius. This choice for the mass model was motivated by the approximately flat rotation curves observed in spiral galaxies and by the analytical tractability of statistical lensing calculations with the SIS model. Statistical lensing calculations using other mass distributions (de Vaucouleurs and King profiles) have been carried out by Dyer (1984). The galactic parameters were, however, poorly known at the time, and little attention was given to magnification bias and to the expected frequency of lensing.

Even though the SIS lens model was motivated by the observed properties of spiral galaxies, all authors agree that early-type galaxies (E and S0), rather than late type, are the dominant type of lens. Much less is known about the existence and properties of halos in early-type galaxies (see, e.g., Kent 1990 for a review). As we will discuss in more detail below, there is at present little observational evidence for or against significant dark matter in early-type galaxies inside a few half-light radii.

In this paper, we carry out a more realistic calculation of statistical lensing of galaxies with and without halos. The properties of the lens galaxies are based on observations: a de Vaucouleurs (1948) surface brightness profile, the "fundamental plane" parameter relations (e.g., Kormendy & Djorgovski 1989), and possible isothermal dark halos, similar to those deduced for spirals. The

[1] Hubble Fellow.

© American Astronomical Society • Provided by the NASA Astrophysics Data System

1993ApJ...416..425M

hypothesized halos have as free parameters their core radii and asymptotic velocities at large radii. We test the importance of extended halos for the expected lensing frequency and the extent to which cosmological inferences are separable from assumptions about the halo properties. The calculation is tailored to the detection limits and sample properties of the *Hubble Space Telescope* (*HST*) snapshot survey for lensed quasars (Bahcall et al. 1992a; Maoz et al. 1992b; 1993a, b). This is the largest published lensing survey of a well-defined sample of quasars. In § 2 we review the properties of spiral and elliptical galaxies and the evidence that stars, rather than dark matter with an isothermal profile, are the dominant mass component in the central few kiloparsecs. In § 3 we outline the lensing calculation. In § 4 we review the observational results from the snapshot survey, and in § 5 we present the statistical methods we use for comparing our model calculations to the observations. In § 6 we present our results, compare them to the observations, study the effects of the main approximations and uncertainties, estimate the completeness of the snapshot survey, and compare our calculation to the SIS model. We briefly summarize our results in § 7.

2. THE STRUCTURE OF GALAXIES AND THEIR HALOS

2.1. *How Important is Dark Matter in Early-Type Galaxies?*

An isothermal density distribution (possibly with a core) can roughly reproduce the flat rotation curves observed in spiral galaxies. The circular velocity can be mapped much more easily in spiral galaxies than in ellipticals, because (1) the emission lines from ionized gas or the 21 cm emission from neutral hydrogen usually extend over a large range in radii and (2) the kinematic tracers are on nearly circular orbits with small random motions, which facilitates the interpretation of the measurement. In many spirals, the three mass components (the bulge, the disk, and the halo) "conspire" to yield an overall flat rotation curve (e.g., Rubin et al. 1985; Bahcall & Casertano 1985; see, however, Casertano & van Gorkom 1991; Persic & Salucci 1991; see Ashman 1992, for a recent review of dark matter in galaxies). In most luminous spirals the halo becomes important only beyond several disk scale lengths, just when the disk mass ceases to sustain the rotation. A typical dark halo core radius for luminous spirals is ~ 12 kpc (Kormendy 1990), with no clear dependence on the Hubble type (Broeils 1992).

Much less is known about the radial run of the circular velocity in early-type galaxies, because in most cases the only available kinematic tracers are stars. In constant to the situation in spirals, the stellar velocities and dispersions in early-type galaxies can only be measured to about the half-light radius, and the interpretation of kinematic data from a "hot" stellar system is complicated by the unknown orbital shapes.

For all but a few ellipticals and S0s, which have special properties, there is no compelling evidence for dark matter. On the other hand, there exist arguments that dark matter is dynamically unimportant over the kinematically probed radial range within about one effective radius r_e.

(1) All existing stellar kinematic data can be fitted with a M/L ratio independent of radius for $r < r_e$; there is no convincing evidence for significant dark matter (e.g., de Zeeuw & Franx 1991, and references therein). Dark matter may become important only at larger radii (see, e.g., Ashman 1992, for a summary).

(2) The central M/L found from stellar kinematics, $M/L_B \sim 10$, agrees with the M/L inferred for the stellar populations from spectral synthesis (Gunn, Stryker, & Tinsley 1981; Bacon 1985; Peletier 1989). Hence, the stellar population producing the light seems to provide all the dynamically inferred mass.

Only for a handful of possibly unrepresentative objects (see Ashman 1992; Franx 1993) does there exist clear evidence that M/L increases toward large radii. This evidence comes either from the properties of an X-ray halo with measurable temperature profile or from H II or H I rings around the galaxy.

One example for the latter is the elliptical galaxy IC 2006, which has a gas ring at large radii. For this ring, a circular velocity of $V = 202$ km s^{-1} is derived by Schweitzer, Van Gorkom, & Seitzer (1989). If this galaxy, with $M_B = -18.24$ mag, has a dark halo with asymptotic velocity dispersion that scales as $\sigma \propto L_B^{0.4}$ (as derived for spirals through the Tully-Fisher relation, e.g., Fukugita et al. 1991), then $\sigma^* \sim 265$ km s^{-1} is implied for the velocity dispersion of the halo of an L^* elliptical. Observations by Franx (1993) of several other such galaxies indicate a similar velocity, and show that for the few special ellipticals, the circular velocity at 5–$10\,r_e$ is comparable to the inferred speed for the inner parts. However, there is no indication whether or not the luminous and dark matter distributions "conspire" to produce a flat rotation curve in the same way that they do in spirals. In fact, if the halos of ellipticals and of spirals of equal luminosity had equal core radii and velocity dispersions, the rotation curves in ellipticals would not be flat. It has been argued that since ellipticals are more concentrated than spirals of equal luminosity, their baryons may have contracted the halo more strongly (Blumenthal et al. 1986; Barnes 1987); in this case, ellipticals could have core radii small enough to yield an overall flat rotation curve.

Most previous calculations of lensing statistics (e.g., TOG; F&T) have implicitly assumed that elliptical galaxies are dominated by dark isothermal mass distributions. The asymptotic velocity dispersion of the dark matter at large radii was estimated from the measured velocity dispersion of the stars at small radii. A correction factor of $(3/2)^{1/2}$ was invoked to account for the different radial density profiles of the stars and the postulated dark matter (Gott 1977). However, one must keep in mind that the inclusion or omission of this factor only implies a rescaling of the rotation curve, which in all cases is assumed to be flat. Some workers (e.g., F&T; Wallington & Narayan 1993) included cores in their isothermal models. The core radius of the isothermal mass distribution was taken to be the observed core radius of the *luminous* matter, which for spirals is more than one order of magnitude smaller than the fitted core radii for their dark halos. Again, the rationale was that the resulting rotation curve from all components was flat at all radii outside the core radius of the luminous material.

In this work, we test the impact on the expected frequency of lensing of the presence of absence of massive halos in early-type galaxies. We also investigate how the halo properties of early-type galaxies are constrained by lensing statistics. We explore the sensitivity of cosmological inferences (e.g., limits on the cosmological parameters Ω and λ) to the details of the assumed lens model.

© American Astronomical Society • Provided by the NASA Astrophysics Data System

1993ApJ...416..425M

2.2. *Mass Models for the Lensing Galaxies*

Much progress has been made in recent years in determining the structural parameters of elliptical galaxies and of the bulges of spiral galaxies. In this subsection, we describe the parameters needed for our lensing calculation. We will treat separately lensing by early-type (elliptical and S0) and late-type (spiral) galaxies.

There are several reasons to treat E's and S0's as a single class. First, the distinction between E's and S0's is viewing angle–dependent, and therefore often lacking in physical basis (e.g., Rix 1991). Second, the presence of the disk is S0s only weakly alters the cumulative mass profile inside the half-mass radius of the bulge. In many S0s, the bulges and disks have similar scale lengths, colors, and contributions to the total light (Rix 1991). The small impact of the disks in S0s on their global parameters can also be judged from parameter relations such as $D_n - \sigma$, which are indistinguishable for E's and S0's (e.g., Faber et al. 1987).

Axisymmetric lenses can be completely specified by the projected cumulative mass profile of the lens, $M(<R)$. In early-type galaxies, we will model this profile with two mass components: (1) a bulge with a radius-independent M/L; (2) an isothermal halo specified by an asymptotic velocity, which scales with galaxy luminosity, and a core radius. The parameters that characterize the bulge (L, M/L, r_e) are drawn from the observed galaxy luminosity function and the "fundamental plane" relations and their projections. The characteristics of the halo are treated as free parameters.

For spiral galaxies, we use the isothermal sphere (IS) approximation to model the mass profile. The IS model is a suitable approximation for spirals since it mimics the generally flat rotation curves that are observed. Since, as has already been shown (e.g., F&T), spirals contribute a small fraction to the total lensing probability, deviations from the IS model will not significantly affect our final results.

All the parameter values we quote are for a Hubble constant value of $H_0 = 100$ km s^{-1} Mpc^{-1}. Since none of our final results depend on H_0, we will not explicitly write H_0 throughout the work. The quoted uncertainties in the parameters are our estimates of the plausible range in these values, and, when possible, were formed from the union of the 1 σ ranges reported by different workers.

2.2.1. *Elliptical and S0 galaxies*

Following F&T, we use the Schechter form of the luminosity function of galaxies, as determined by Efstathiou, Ellis, & Peterson (1988, hereafter EEP):

$$\phi_g(L)dL = \phi^*\left(\frac{L}{L^*}\right)^{\alpha} e^{-L/L^*}\frac{dL}{L^*}, \tag{1}$$

with

$$\phi^* = (1.56 \pm 0.4) \times 10^{-2}\ \mathrm{Mpc}^{-3}, \tag{2}$$

$$\alpha = -1.1 \pm 0.1, \tag{3}$$

and

$$M^*(B_T^0) = -19.9^{-0.2}_{+0.4}. \tag{4}$$

$M^*(B_T^0)$ is the absolute blue magnitude associated with a luminosity L^*. Like F&T, we take the fraction of elliptical and S0 galaxies to be

$$f_{\mathrm{E+S0}} = 0.31 \pm 0.05. \tag{5}$$

The projected surface brightness profiles $I(r)$ of both ellipticals and the bulges of spirals can be described by de Vaucouleurs's (1948) empirical law:

$$I(r) = I(r_e)e^{-7.67(r/r_e)^{1/4}}, \tag{6}$$

where r_e is the effective radius enclosing half the total light. Modern CCD surface photometry (e.g., Jorgensen, Franx, & Kjaergaard 1992) reconfirms that this functional form usually fits well the observed profiles.

An important breakthrough in the study of the structural parameters of galaxies occurred with the realization that elliptical galaxies lie in a thin inclined plane ("the fundamental plane") in the three-parameter space of luminosity, effective radius, and velocity dispersion (or other combinations of these parameters). Reviews of the fundamental plane and other properties of ellipticals can be found in Faber et al. (1987), Kormendy & Djorgovski (1989), and de Zeeuw & Franx (1991).

A projection of the fundamental plane onto the $L - r_e$ plane indicates that the effective radius grows faster than the square-root of the luminosity L, so that more luminous galaxies have lower mean surface brightness. This relation can be described by a power-law relation

$$r_e = r_e^*(L/L^*)^a, \tag{7}$$

where r_e^* is the effective radius of an L^* galaxy. Although the scatter is this relation can be lowered by introducing an additional variable (e.g., the central velocity dispersion σ), the $L - r_e$ correlation is in itself fairly tight, and is therefore useful for relating a realistic r_e to a given L (see, e.g., Sodré & Lahav 1993; in § 6.4.2 we will examine the effect of, more realistically, deriving L and r_e from a bivariate distribution). From work by de Carvalho & da Costa (1988), Kormendy & Djorgovsky (1989), Rix (1991), and Jorgensen et al. (1992), we estimate

$$a = 1.2 \pm 0.3, \tag{8}$$

$$r_e^* = 4 \pm 1\ \mathrm{kpc}. \tag{9}$$

© American Astronomical Society • Provided by the NASA Astrophysics Data System

1993ApJ...416..425M

The tightness and slopes of the fundamental plane, coupled with the virial theorem, indicate that the central M/L ratios also depend on luminosity:

$$M/L = (M/L)^*(L/L^*)^b \,. \tag{10}$$

From Faber et al. (1987), Kormendy & Djorgovsky (1989), and van der Marel (1991), we take

$$b = 0.25 \pm 0.10 \,, \tag{11}$$

$$(M/L_B)^* = 10 \pm 2 \,, \tag{12}$$

with b having a possible dependence on metallicity. For $(M/L)^*$ we have used the results of van der Marel (1991), who employed major and minor axis fitting of two integral models to a sizeable set of elliptical galaxies to obtain M/L estimates. These estimates are the only available ones that take the flattening of the galaxies and their rotation properly into account. Once the dependence of M/L on luminosity is included, the residuals about equation (10) do not correlate with any other structural parameter (e.g., rotation and isophote shapes) at the $\lesssim 20\%$ level. We therefore assume 20% to be a reasonable estimate for the errors in the mean M/L.

As already noted, all existing data can be explained by assuming the M/L ratio in the central regions of a given galaxy is independent of radius. This implies that the projected surface mass density is proportional to the surface brightness:

$$\Sigma(r) = (M/L)I(r) \,. \tag{13}$$

By combining equations (7), (10), and (13), we find that the mean surface mass density for a galaxy of luminosity L is

$$\Sigma_{\rm av} = \Sigma^*_{\rm av}(L/L^*)^{1-2a+b} \,. \tag{14}$$

The values of the parameters given above yield

$$\Sigma^*_{\rm av} \equiv \frac{L^*}{2\pi r_e^{*2}}\left(\frac{M}{L}\right)^* = 0.3^{+0.4}_{-0.1}\ {\rm g\ cm^{-2}} \,. \tag{15}$$

As explained in the previous section, there is little information regarding the dark halos of early-type galaxies. We will attempt to use the observed statistics of lensing to constrain the velocity dispersions σ, core radii r_c, and scaling law with luminosity of the halos of early-type galaxies. Our parameterization will be

$$\sigma = \sigma^*(L/L^*)^c \,, \tag{16}$$

and

$$r_c = x_c\, r_e \,, \tag{17}$$

with x_c a constant. σ^*, r_c, and c will be treated as free parameters. The power-law relation between velocity dispersion and luminosity is motivated by the observations of this relation in the dark halos of spiral galaxies. The assumption that the dark matter core radius is proportional to the effective radius of the light gives the simplest parameterization that is consistent with the kinematic observations (e.g., if r_c were constant, galaxies with $r_e > r_c$ would have a M/L ratio that increased with radius). More complicated functional dependences for r_c are, of course, possible but would introduce additional free parameters.

2.2.2. *Spiral Galaxies*

About 70% of galaxies are spirals and irregulars (e.g., Postman & Geller 1984). The mass distribution of spiral galaxies is conventionally described in terms of three components: a bulge, a disk, and a dark isothermal halo with a core size $\gtrsim 10$ kpc for an L^* galaxy (e.g., Broeils 1992). Multicomponent fits show that in the inner few kpc, the mass is dominated by the bulge of the galaxy, with the dark halo contributing only a small fraction.

Kent (1985) and Simien & de Vaucouleurs (1986), have carried out bulge/disk decompositions for large samples of spiral galaxies. They find that the fractional luminosity of the bulges is independent of luminosity, and decreases from $\sim 40\%$ in early spiral galaxy types (Sa–Sab) to less than $\sim 10\%$ in late-type galaxies (Sc and later). Since EEP show that spirals of type Sa–Sbc follow the same Schechter luminosity function as ellipticals, this suggests that the luminosities of the *bulges* of Sa–Sbc galaxies also have a Schechter distribution, but with a characteristic luminosity $\lesssim 0.6L^*$. EEP find that later type galaxies (Sc–I) are considerably fainter than early-type galaxies, with $M^*_{\rm Sc} \sim -19.0$. Since such galaxies have at most 20% of their light in their bulges, it follows that their bulges have a characteristic luminosity $< 0.1L^*$. We will assume that half of spirals are Sa–Sbc and half are Sc and later.

From Kent's (1985) data we see that the bulges of Sa and Sab galaxies appear to follow the relation between luminosity and effective radius determined for ellipticals and S0's. Later types are progressively less concentrated, so that the effective radius of the bulge of a spiral is always larger than that of an elliptical galaxy of the same luminosity. The elliptical galaxy effective radius can therefore be considered as a lower limit.

Spirals have rotation curves that rise in their inner regions and then remain approximately flat out to the largest radii that can be measured. For our purposes, this gross rotation-curve behavior can be mimicked by a one-component model consisting of an isothermal halo with a core radius of $0.16r_e$, with r_e the effective radius of the bulge. For a de Vaucouleurs bulge with effective radius r_e, the maximum in the rotation curve occurs at $0.16r_e$ (see § 3, below). We therefore model spiral galaxies as isothermal spheres having core radii proportional to the bulge effective radius. The bulge effective radii are determined from equation (7) using the bulge luminosity. At large radii, we follow F&T and, based on the B-band Tully-Fisher relation (Freedman 1990; Fukugita et al. 1991), take the asymptotic velocity dispersion of the isothermal sphere to be

$$\sigma = \sigma^*(L/L^*)^d \,, \tag{18}$$

© American Astronomical Society • Provided by the NASA Astrophysics Data System

1993ApJ...416..425M

with

$$d = 0.38 \pm 0.04 , \tag{19}$$

and

$$\sigma^* = 144^{+8}_{-13} \text{ km s}^{-1} . \tag{20}$$

3. LENSING CALCULATIONS

In this section we outline the lensing calculation. Our work supersedes previous such calculations in that we use the most realistic surface mass distributions, namely, those implied by observations. Our main approximation is the assumption that lenses are cylindrically symmetric mass distributions. This approximation greatly simplifies the calculation. Blandford & Kochanek (1987) and Kochanek & Blandford (1987) have shown that departures from cylindrical symmetry cause a fraction of the lenses, of order of the square of the ellipticity of the potential, to have five-image configurations rather than the three-image configuration that a circular lens gives. The ellipticity of the lensing potential has, however, little effect on the lensing cross section of a galaxy, or on the expected distribution of image separations, which are dominated by the monopole of the lensing potential (Kochanek 1992). In § 6, we return to study the effect on our results of several other approximations we will now make: the approximations that spiral galaxies are unimportant; that lensing galaxies are always isolated (rather than being in clusters sometimes); and that there is a perfect relation between effective radius and luminosity (eq. [7]).

3.1. *The Lensing Equation*

A light ray passing with an impact parameter b from the center of a cylindrically symmetric mass distribution is bent by an angle

$$\alpha = \frac{4GM(<b)}{c^2 b} , \tag{21}$$

(e.g., Weinberg 1972), where $M(<b)$ is the total mass that is projected inside of b. The lensing equation, relating the angle θ_I between the lens and the projected image to the angle θ_S between the source and the lens, is

$$\theta_S = \frac{D_{\rm LS}}{D_{\rm OS}} \alpha(\theta_I) - \theta_I , \tag{22}$$

where $D_{\rm LS}$ and $D_{\rm OS}$ are the angular diameter distances between the lens and the source and between the observer and the source, respectively. The condition for gravitationally lensing a source into multiple images is that the source be projected on the sky within an angle $\theta < \theta_{\rm cr}$ of the lens,

$$\theta_{\rm cr} = \frac{D_{\rm LS}}{D_{\rm OS}} \alpha(\theta_I) - \theta_1 , \tag{23}$$

where θ_1 is defined by

$$\left. \frac{D_{\rm LS}}{D_{\rm OS}} \frac{d\alpha}{d\theta} \right|_{\theta=\theta_1} = 1 . \tag{24}$$

For a lensing galaxy with constant mass-to-light ratio M/L and any surface brightness profile $I(r)$ with effective radius r_e (that encloses half the total light), equation (21) can be rewritten as:

$$\alpha = \frac{4G(M/L)L}{2c^2 r_e} f(x) , \tag{25}$$

with the dimensionless function $f(x)$ defined as

$$f(x) \equiv \frac{1}{x} \frac{\int_0^x I(r) r \, dr}{\int_0^1 I(r) r \, dr} , \tag{26}$$

and

$$x \equiv \frac{b}{r_e} . \tag{27}$$

Combining equations (23) and (25), we can write the critical radius for lensing as

$$r_{\rm cr} = r_e \left[\frac{\Sigma_{\rm av}}{\Sigma_{\rm cr}} f(x_1) - x_1 \right] . \tag{28}$$

Here $\Sigma_{\rm av}$ is the mean surface mass density inside r_e (eq. [15]), $\Sigma_{\rm cr}$ is the critical surface mass density, defined as

$$\Sigma_{\rm cr} \equiv \frac{c^2}{4\pi G} \frac{D_{\rm OS}}{D_{\rm OL} D_{\rm LS}} , \tag{29}$$

© American Astronomical Society • Provided by the NASA Astrophysics Data System

1993ApJ...416..425M

where D_{OL} is the angular diameter distance from the observer to the lens, and $x_1 = D_{OL}\theta_1/r_e$, so that, from equation (24),

$$\left.\frac{df}{dx}\right|_{x_1} = \frac{\Sigma_{cr}}{\Sigma_{av}} . \tag{30}$$

Using a de Vaucouleurs surface brightness profile $I(r)$ (eq. [6]), we integrate equation (26) and find

$$f(x) = \frac{1}{2520x}\left[e^q(q^7 - 7q^6 + 42q^5 - 210q^4 + 840q^3 - 2520q^2 + 5040q - 5040) + 5040\right] , \tag{31}$$

where $q \equiv -7.67x^{-1/4}$.

An isothermal halo with asymptotic velocity dispersion σ and core radius r_c has a mass interior to b that can be approximated (e.g., Hinshaw & Krauss 1987) as

$$M(<b) = \pi\sigma^2[(b^2 + r_c^2)^{1/2} - r_c]/G . \tag{32}$$

The critical radius for a mass distribution composed of the superposition of a de Vaucouleurs bulge and an isothermal halo is

$$r_{cr} = r_e\left[\frac{\Sigma_{av}}{\Sigma_{cr}} f(x_1) + \frac{\sigma^2}{\Sigma_{cr} G r_e} h(x_1) - x_1\right] , \tag{33}$$

where

$$h(x) = [(x^2 + x_c^2)^{1/2} - x_c]/x , \tag{34}$$

and x_1 now obeys

$$\frac{\Sigma_{av}}{\Sigma_{cr}}\left.\frac{df}{dx}\right|_{x_1} + \frac{\sigma^2}{\Sigma_{cr} G r_e}\left.\frac{dh}{dx}\right|_{x_1} = 1 . \tag{35}$$

Using the structural relations for elliptical galaxies in § 2 (eqs. [7], [10], and [14]), we can write the critical radius as a function of luminosity:

$$r_{cr} = r_e^*\left(\frac{L}{L^*}\right)^a\left[\frac{\Sigma_{av}^*}{\Sigma_{cr}}\left(\frac{L}{L^*}\right)^{1-2a+b} f(x_1) + \frac{\sigma^{*2}}{\Sigma_{cr} G r_e^*}\left(\frac{L}{L^*}\right)^{2c-a} h(x_1) - x_1\right] . \tag{36}$$

We show in Figure 1 the functions $f(x)$ and $h(x)$ for a de Vaucouleurs law and isothermal halos with cores of various sizes, and the sums of the two mass components. Determining the critical radius for a galaxy of given luminosity involves solving numerically the polynomial equation (35) for x_1 and substituting x_1 into equation (33).

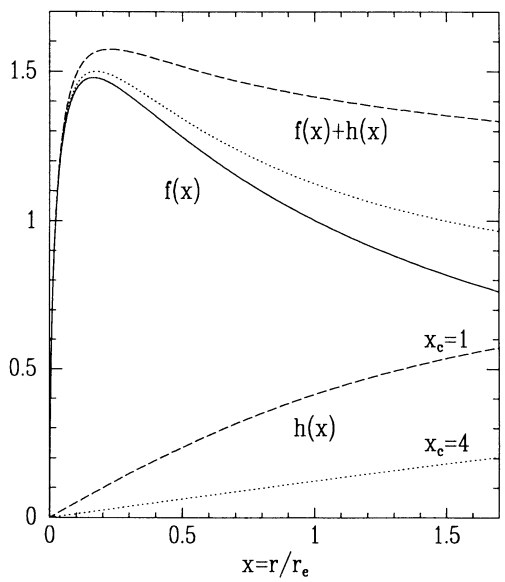

FIG. 1.—Bend angle curve for de Vaucouleurs galaxies with and without isothermal halos. The solid curve shows the bending angle of a de Vaucouleurs surface mass profile, $f(x)$ (eq. 31), and the lower dashed and dotted lines show that of two isothermal halos with different cores sizes, $h(x)$ (eq. 34). The top dashed and dotted curves show the bending angle of the combined galaxy-halo system. Note that the location and height of the maximum changes little, as does the location of unit derivative; hence, the addition of a halo hardly changes the lensing cross section. The important difference is the extent to which the function drops off outside its maximum, because this affects both the typical image separation and the magnification bias.

© American Astronomical Society • Provided by the NASA Astrophysics Data System

1993ApJ...416..425M

As outlined in the previous section, we model spiral galaxies using only an isothermal halo component $h(x)$, but with $r_c = 0.16r_e$, where r_e is the effective radius of the bulge. This mass model can mimic the observed rotation curves of spirals, which rise in the inner regions of the galaxy and then remain approximately flat. The asymptotic velocity dispersion is found from the Tully-Fisher relation in equation (18).

Whenever the source is projected within r_{cr} it will be lensed into three images, one on the same side of the lens as the source, and two on the opposite side. In practice, one or both of the images on the opposing side often become highly demagnified, and thus undetectable, at projected radii smaller than r_{cr}. Furthermore, all image pairs among the three images may have angular separations smaller than the observational resolution limit. We will therefore be concerned with the *observational* critical radius, defined as the maximal radius at which the source can be projected from the lens and still form *detectable* multiple images. This radius will obviously depend on the survey under consideration.

3.2. *Detection Limits, Magnification Bias, and Cross Sections*

Bahcall et al. (1992a) and Maoz et al. (1992b) estimated the multiple-image detection limits of the snapshot survey using blind simulations. The detection function is well described by the following form:

$$D(A_1/A_2, \Delta\theta) = \begin{cases} 1\,, & \text{for } A_1/A_2 < 19(\Delta\theta)^{0.85}\,, \\ 0\,, & \text{for } A_1/A_2 > 19(\Delta\theta)^{0.85}\,, \\ 0\,, & \text{for } A_1/A_2 > \min\,(40, K)\,, \quad \text{or } (\Delta\theta) < 0''.1\,, \end{cases} \tag{37}$$

where A_1/A_2 is the amplification ratio of a bright to a faint image, $\Delta\theta$ is the angular separation between the two images in arc seconds, and K is the ratio between the brightness of the object and the faint detection limit of the exposure, which we take as $V = 22$ mag.

The magnification bias is an enhancement of the probability that a quasar of given magnitude is lensed. The bias is due to the lensing amplification of intrinsically fainter quasars to the observed quasar magnitude (TOG; F&T). While in the SIS approximation the bias depends only on the redshift and magnitude of the quasar, in the general case it depends also on the properties of the lens (i.e., its luminosity and redshift) and on the detection limits. The bias for a quasar of redshift z and B-band luminosity L_Q can be written as:

$$B(L_Q, z) = \frac{\int_0^\infty \phi_Q(L_Q/A, z)P(A)dA\, d(L_Q/A)}{\phi_Q(L_Q, z)dL_Q}\,. \tag{38}$$

$P(A)dA$ is the probability that a detectable multiple imaging event will cause a total flux increase by a factor A, and $\phi_Q(L_Q, z)$ is the quasar luminosity function of quasars of redshift z. Note that this formula is equivalent to the one given by F&T in magnitude form (rather than amplification form). It is also the same as that given by TOG. The statement by F&T that TOG have an erroneous factor of A^{-1} is incorrect.

As in Bahcall et al. (1992a) and in subsequent snapshot survey papers, we use the Boyle et al. (1987) quasar luminosity function for redshifts $z < 3$:

$$\phi_Q(L_Q, z) = \phi_Q^*(L_Q/L_Q^*)^\alpha\,, \qquad L_Q < L_Q^*\,; \tag{39}$$

$$\phi_Q(L_Q, z) = \phi_Q^*(L_Q/L_Q^*)^\beta\,, \qquad L_Q > L_Q^*\,. \tag{40}$$

L_Q^* is the luminosity of the break in the luminosity function and depends on redshift as

$$L_Q^*(z) = L_{Q0}^*(1 + z)^{k_L}\,. \tag{41}$$

The values of the parameters introduced above are

$$\alpha = -1.2 \pm 0.2\,, \tag{42}$$

$$\beta = -3.6 \pm 0.2\,, \tag{43}$$

$$M_{Q0}^* = -20.25 \pm 0.5\,, \tag{44}$$

$$k_L = 3.5 \pm 0.3\,, \tag{45}$$

where M_{Q0}^* is the B-band absolute magnitude corresponding to L_{Q0}^*. For redshifts $z > 3$ we adopt a behavior of the luminosity function similar to that assumed by Wallington & Narayan (1993): the slopes below and above the break in the luminosity function remain as they were before, but the break "slides down" along the high-luminosity part, so that

$$L_Q^*(z) = L_{Q0}^*\,4^{k_L}3.2^{z-3}\,. \tag{46}$$

Maoz et al. (1993a) tabulated for each snapshot survey quasar the absolute magnitude M_V, derived from its observed V magnitude, as measured in the snapshot observations. Since most of the quasars in the snapshot sample do not have measured B-band magnitudes, we transform M_V to a B magnitude using a typical quasar rest frame $B - V = 0.2$.

© American Astronomical Society • Provided by the NASA Astrophysics Data System

1993ApJ...416..425M

For many lens mass distributions, the total image amplitude amplification $A(r)$ resulting from a projected lens-source separation r can be parameterized as

$$A = A_{\rm min}(r/r_{\rm cr})^{1/\gamma}\,, \tag{47}$$

with $\gamma < 0$. In the SIS case, $A_{\rm min} = 2$, and $\gamma = -1$ for all A. It can be shown (Kovner 1987) that for all circular lenses, γ approaches -1 for large A. The probability of amplification A is

$$P(A) = -2\gamma A_{\rm min}^{-2\gamma} A^{2\gamma-1} \tag{48}$$

Defining $A^* \equiv L_Q/L_Q^*$, we can integrate equation (38) for $\gamma < (\alpha+1)/2 < 0$ to obtain

$$B = \begin{cases} -2\gamma A_{\rm min}^{-2\gamma} A^{*(2\gamma-\beta-1)}\left(\dfrac{1}{2\gamma-\beta-1} - \dfrac{1}{2\gamma-\alpha-1}\right) + \dfrac{2\gamma A_{\rm min}^{-\beta-1}}{2\gamma-\beta-1}\,, & A^* > A_{\rm min}\,; \\ \dfrac{2\gamma A^{*(\alpha-\beta)} A_{\rm min}^{-\alpha-1}}{2\gamma-\alpha-1}\,, & 1 < A^* < A_{\rm min}\,; \\ \dfrac{2\gamma A_{\rm min}^{-\alpha-1}}{2\gamma-\alpha-1}\,, & A^* < 1\,. \end{cases} \tag{49}$$

We note that there have recently been reports that the quasar luminosity function has not been accurately determined, even at low redshift. Goldschmidt & Miller (1991) find that a large fraction of high-luminosity quasars has been missed by previous surveys. The slope at high luminosities may then not be as steep as previously thought, which would have the effect of reducing the magnification bias. Majewski et al. (1991) find that, by surveying for quasars by means of variability and lack of proper motions, they discover a population of quasars having stellar colors that is missed by UV-excess surveys. In this case, however, the revision of the quasar luminosity function would not affect the bias calculation, unless lensing can somehow transform some of these red quasars into UV-excess quasars *and* the two populations have different luminosity function shapes. Several ongoing quasar surveys may soon help clarify whether the quasar luminosity function needs to be revised, in which case our results in this work might be modified.

The probability that a quasar is lensed is found by integrating the cross section for a single lens, $B\pi r_{\rm cr}^2$, where $r_{\rm cr}$ is the observational critical radius, over the galaxy luminosity function and over all redshifts between the observer and the quasar. If we assume a constant comoving density of galaxies, then the probability is

$$\tau = \int_0^{z_Q} dz\,\frac{c\,dt}{dz}\,(1+z)^3 \int_0^{\infty} dL\,\phi_g(L) B\pi r_{\rm cr}^2\,. \tag{50}$$

The expected number of quasars that are lensed by a galactic population ϕ_g is the sum over the individual lensing probabilities of the quasars in the sample. The distribution of angular separations can be found by summing the suitably weighted distributions due to each of the individual lenses in the calculation.

The angular diameter distances involved in the calculation depend on the choice of cosmology. We examine several cases: an empty universe ($\Omega_0 = 0$), a flat ($k = 0$) universe ($\Omega_0 = 1$), and flat universes with a cosmological constant [$\Omega_0 + \lambda = 1$, where $\lambda \equiv \Lambda/(3H_0^2)$ is the dimensionless form of the cosmological constant Λ]. In the flat cases we use the filled beam approximation (see, e.g., TOG; Krauss & White 1992). Defining $w \equiv 1 + z_{\rm lens}$ and $y \equiv 1 + z_{\rm quasar}$, the formulae we use are as follows.

For $\Omega = 0$:

$$\frac{D_{\rm LS}}{D_{\rm OS}} = \left(1 - \frac{y^2}{w^2}\,\frac{w^2-1}{y^2-1}\right), \tag{51}$$

$$D_{\rm OL} = \frac{c}{H_0}\,\frac{w^2-1}{2w}\,, \tag{52}$$

$$\frac{c\,dt}{dw} = \frac{c}{H_0}\,w^{-2}\,. \tag{53}$$

For $\Omega_0 = 1$:

$$\frac{D_{\rm LS}}{D_{\rm OS}} = \left(1 - \frac{y^{0.5}}{w^{0.5}}\,\frac{w^{0.5}-1}{y^{0.5}-1}\right), \tag{54}$$

$$D_{\rm OL} = \frac{c}{H_0}\,\frac{w^{0.5}-1}{w^{1.5}}\,, \tag{55}$$

$$\frac{c\,dt}{dw} = \frac{c}{H_0}\,w^{-2.5}\,. \tag{56}$$

© American Astronomical Society • Provided by the NASA Astrophysics Data System

1993ApJ...416..425M

For $\Omega_0 + \lambda = 1$:

$$\frac{D_{LS}}{D_{OS}} = \frac{\chi_Q - \chi_L}{\chi_Q}, \tag{57}$$

$$D_{OL} = \frac{c}{H_0}\frac{\chi_L}{w}, \tag{58}$$

$$\frac{c\,dt}{dw} = \frac{c}{H_0}\frac{1}{w(\Omega_0 w^3 - \Omega_0 + 1)^{1/2}}, \tag{59}$$

where

$$\chi_L = \int_1^w \frac{dw'}{(\Omega_0 w'^3 - \Omega_0 + 1)^{1/2}} \tag{60}$$

and

$$\chi_Q = \int_1^y \frac{dw'}{(\Omega_0 w'^3 - \Omega_0 + 1)^{1/2}} \tag{61}$$

are the comoving distances to the lens and the source, respectively.

3.3. *Numerical Calculation*

Using the relations given in the previous section, we carry out the following numerical calculation: for a galaxy of luminosity L and a quasar of absolute magnitude M_V and redshift z, we determine the scaled critical radius $x_{cr} = r_{cr}/r_e$ by solving for x_1 in equations (30) or (35). From the lensing equation we then find the three image positions and amplifications for every $x < x_{cr}$ and, using the detection function (37), determine the observational x_{cr} within which at least one image pair is detectable. For all lens mass distributions we consider, $A(r)$ can be approximated by a power law over most of the range in r. The power-law slope and normalization [$1/\gamma$ and A_{min} in eq. (47)] are found by calculating the total amplification at $0.2x_{cr}$ and $0.9x_{cr}$ (see next section). A^* and the magnification bias are then computed from equation (49). The lensing cross section due to galaxies of that luminosity is calculated by weighting πr_{cr}^2 by the galaxy luminosity function ϕ_g for a particular class of galaxies and by the magnification bias B. The calculation is repeated, and the cross section is summed, over a grid of galaxy luminosities from $0.05L^*$ to $4L^*$, and over a grid of lens redshifts from 0 to z_Q, according to equation (50). We thus obtain the probability that the given quasar is lensed and the distribution of image separations that the lenses produce. The numerical procedure is repeated for every quasar in the snapshot sample and the probabilities and distributions are summed in order to obtain the sample lensing statistics predicted by a particular model.

4. THE SNAPSHOT SURVEY OBSERVATIONS

In this section we review the observational results of the *HST* snapshot survey. The snapshot survey yields two observables that can be compared directly with our calculations: the total number of lensed quasars and the distribution of angular image separations. A third observable, the distribution of relative image amplifications, is difficult to compare with the predictions of circular symmetric lenses, which never produce five-image configurations. Furthermore, even in detailed (noncircular) models of individual lenses, the image brightness ratios are hard to reproduce due to the effects of extinction by dust and/or microlensing in the lensing galaxy (e.g., Rix, Schneider, & Bahcall 1992). The distribution of lensing galaxy redshifts is, in principle, another observable (Kochanek 1992). The redshifts of the lenses in the snapshot sample are, however, either unknown or poorly known (e.g., Kochanek 1991a). We will test our model predictions against the total observed number of lenses and their angular distribution and investigate to what degree these two observables have a separable dependence on the parameters of the model.

As summarized by Maoz et al. (1993a), the snapshot sample of 502 quasars includes the following six lens candidates, in order of increasing maximum image separations:

1208+1011—0.″47 separation;
1413+117—1.″22 separation;
1115+080—2.″0 separation;
0142−100—2.″2 separation;
0957+561—5.″7 separation;
1120+0154—6.″6 separation.

(For the four-image lenses, 1413+117 and 1115+080, we have listed the geometrical mean of the separations of the two diagonal pairs.) The last two objects have much larger image separations than the other four. In the case of 0957+561 it is known that one or two clusters of galaxies, in addition to a brightest cluster galaxy, are responsible for the lensing (Young et al. 1981). Recently, Bernstein, Tyson, & Kochanek (1993) have shown that 0957+561 is a highly complex system that is difficult to model, even with many free parameters. As we will see below, even if the effect of clusters is taken into account, our calculations always predict that lens systems with such large image separations are exceedingly rare. In order to proceed, we will assume that the existence of the 0957+561 lens system is a statistical fluke, similar to the existence of the lens system 2237+0305, which is also highly unlikely. Our assumption is problematic if 1120−0154 is also a lensed quasar. In the case of 1120+0154, however, there is also some doubt as to

© American Astronomical Society • Provided by the NASA Astrophysics Data System

1993ApJ...416..425M

whether we are dealing with a real lens system rather than a physical pair. The ambiguity results from the unusually larger separation coupled with the absence of any obvious lensing galaxy or cluster and possible small differences in the spectra of the two components. We will therefore not include 0957+561 and 1120+0154 in our comparison between observations and models.

Among the remaining four lenses, 1208+1011, which was discovered by the snapshot survey (Maoz et al. 1992a; Magain et al. 1992), is probably a lensed quasar (Bahcall et al. 1992b, c). However, the observational results are not yet precise enough to make a definitive test of the lensing hypothesis for this object. We consider 1208+1011 to be lensed for the purpose of this analysis. Should 1208+1011 turn out to be a physical pair of quasars, a dearth of subarcsecond lenses would be implied.

5. LIKELIHOOD ESTIMATES FOR THE MODELS

In this section we present statistical methods for comparing the models and the observations, which we use in the next sections to test a variety of models. Each model with a set of parameters (e.g., Ω, r_e^*, r_c,...) predicts a number distribution, $n(\theta)$, for the separations of multiple images. The integral over this distribution, $N \equiv \int_0^\infty n(\theta)d\theta$, yields the expected number of quasars with observable split images. The relative likelihood of various models can be calculated as follows.

Suppose the observed separations, θ, were placed in small bins $\delta\theta$, such that the probability p_i of finding a system in the ith bin with $(i-1)\cdot\delta\theta < \theta < i\cdot\delta\theta$ is small for all i. The likelihood function for any model can be defined as

$$L \equiv \sum_{\text{all bins}} \ln(p_i) , \tag{62}$$

with

$$p_i \equiv \frac{n(\theta_i)^{n_i} e^{-n(\theta_i)}}{n_i!} \tag{63}$$

where n_i is the number of observed systems in bin i. Since n_i is either 1 or 0, eq. (62) simplifies to

$$L = \left[\sum_{n_i>0} \ln n(\theta_i)\right] - N . \tag{64}$$

Thus the likelihood is just a sum over the few bins in which systems are observed and can be easily evaluated for any $n(\theta)$ produced by a set of parameters. In principle, the most likely set of parameters can be found by maximizing L over all of parameter space. In practice, it is difficult to present the likelihood as a high-dimensional function of all parameters. To illustrate the sensitivity of the model likelihood to various parameters we will therefore present it as a one- and two-dimensional function for various parameters, with all other parameters fixed at some fiducial value. This relative likelihood estimate, however, does not provide a measure of the absolute likelihood of any given model.

In order to test for consistency in an absolute sense (i.e., answer questions such as, "Is a given model compatible with the observations?") we can draw Monte Carlo realizations of the observations from $n(\theta)$ and calculate the distribution of simulated likelihoods for this model. Then we can ask in which fraction of simulated observations we get a likelihood as low as observed.

6. RESULTS AND COMPARISON WITH OBSERVATIONS

In this section we present the results of our calculations and compare them to the snapshot survey observations. We first treat pure de Vaucouleurs lenses, i.e., lenses without isothermal halos. In order to elucidate the numerical results, we describe the results of the various stages of the calculation outlined above and compare the result of each stage to the SIS results.

6.1. *Lensing by Early-Type Galaxies Without Halos*

6.1.1. *Qualitative Behavior*

Equation (28) shows that the critical radius r_{cr} depends in a nontrivial way on the luminosity. Figure 2 shows, in an $\Omega = 1$ cosmology, r_{cr} as a function of lens luminosity of de Vaucouleurs lenses at redshift 0.5 and a quasar at redshift 2.0. For comparison, we also show (*dashed line*) r_{cr} for the SIS model, which is proportional to $L^{1/2}$. Unlike the SIS model, the de Vaucouleurs r_{cr} has a weak dependence on luminosity. The behavior of the de Vaucouleurs r_{cr} is due to the decrease in mean surface density in brighter galaxies. The break in the curve at $0.35L^*$ (for $a = 1.2$) and the decrease in r_{cr} at lower luminosities are produced by the detection limits: although multiple images are in principle being formed at large impact parameters, the two inner images are too highly demagnified to be detected. Coincidentally, the low-luminosity part of the curve lies close to the SIS curve. The luminosity of the break in the curve of Figure 2 and the slopes of the curve depend on the parameters a and b in equations (7) and (10). From the first term in equation (33), we see that at low luminosities, x_1 and $f(x_1)$ approach constant values [namely, 0.16 and $f(0.16)$, respectively; see Fig. 1], so that

$$r_{cr} \sim L^{1-a+b} . \tag{65}$$

For example, for a value of $a = 0.75$ (rather than the $a = 1.2$ we have adopted) and $b = 0.25$, $r_{cr} \sim L^{0.5}$, as in the SIS case. By adopting a smaller r_e^* than we have chosen (2.5 kpc instead of 4.0 kpc), one can also raise the normalization of the de Vaucouleurs r_{cr} curve and have it match well the SIS curve at all luminosities. One might naively expect that, with the certain freedom in the choice of a and r_e^*, the predictions of the two models can be made to match. We find, however, that the effect of the parameters on the cross sections and on the magnification bias is opposite and therefore cancels in the observable quantities.

Figure 3 shows the magnification bias as a function of luminosity. The qualitative behavior of the magnification bias can be understood as follows. In the SIS case, the minimum amplification A_{min} is always 2. In the de Vaucouleurs case, the decrease in $f(x)$

© American Astronomical Society • Provided by the NASA Astrophysics Data System

1993ApJ...416..425M

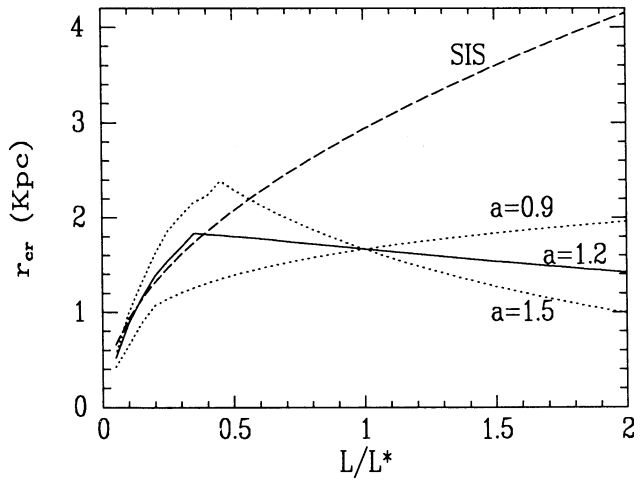

FIG. 2

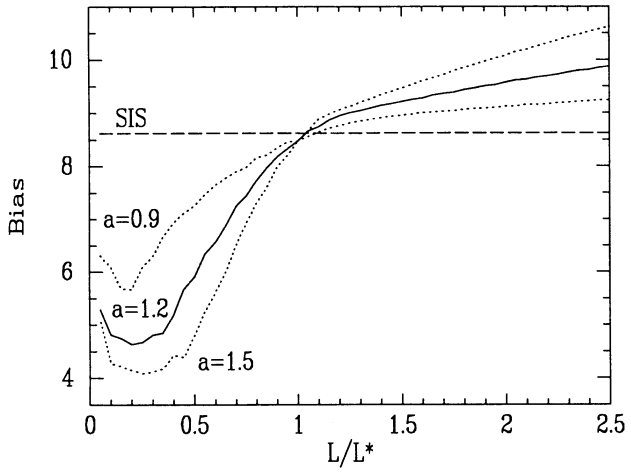

FIG. 3

FIG. 2.—Observational critical radius of de Vaucouleurs lenses as a function of lens luminosity, for $z_{lens} = 0.5$, $z_{quasar} = 2.0$. While the singular isothermal sphere (SIS, *dashed curve*) has a simple $L^{1/2}$ dependence, the critical radius for the Vaucouleurs galaxies depends both on the assumed r_e vs. L relation and on the detection function of the lens survey. The solid and dotted curves show $r_{cr}(L)$ for a range of luminosity-radius power law relations (see eq. 7). The downturn of these curves at low luminosity is caused by the demagnification of two of the three images to beyond the limits of the survey.

FIG. 3.—Magnification bias of de Vaucouleurs lenses as a function of lens luminosity, for $z_{lens} = 0.5$, $z_{quasar} = 2.0$, and quasar absolute magnitude $M_V = -25.5$. Low-luminosity galaxies have more concentrated light (mass) distributions than luminous galaxies, and thus have a more steeply falling bend angle with increasing impact parameter. This results in lower minimum total amplification A_{min} and hence lower magnification bias for the less luminous galaxies. The dependence on a, the power-law index relating the effective radius r_e and luminosity, is in the opposite sense to the dependence of r_{cr} on a (Fig. 2). The product of bias and r_{cr}^2 therefore depends weakly on a (see Fig. 4*a*). Also shown is the bias in the SIS approximation, which is independent of lens luminosity.

for $x > 0.16$ means that, for lenses with high Σ_{av}/Σ_{cr}, the image that is projected on the same side as the source can be close to the source position. The magnification can therefore approach unity. Alternatively, lower density lenses have small r_{cr}/r_e, and the minimum amplification that is obtained when the source is near the critical radius can be larger than 2. We find that

$$A_{min} \propto L^{a-b} . \tag{66}$$

The slope $1/\gamma$ of equation (47) is close to -1, as expected, for large amplifications, i.e., at $x \lesssim 0.2x_{cr}$. At larger x, the slope depends on the luminosity of the galaxy, so that luminous galaxies, which have high amplifications, have $1/\gamma \sim -1$, while fainter galaxies can have $1/\gamma \sim -0.8$. As x approaches x_{cr}, $1/\gamma$ becomes flatter due to the increasing amplification of the two merging images at the opposed side of the source. Because the merging occurs at low total amplification, it has little effect on $P(A)$ (and in fact makes low amplifications somewhat more probable and therefore high amplifications less probable). In most of the range of x, corresponding to most of the area inside x_{cr}, the power-law slope γ is approximately constant. For every lens, we therefore determine γ between $0.2x_{cr}$ and $0.9x_{cr}$. The fact that A_{min} can be less than 2 and $1/\gamma$ shallower than -1 means that the probability of high amplification and therefore, the magnification bias, are smaller than in the SIS case. Since γ is generally close to -1, then from equations (49) and (68), $B \sim A_{min}^2 \sim L^{2a-2b}$. On the other hand, from equation (71), $r_{cr} \propto L^{1-a+b}$. Thus the cross section for lensing, $B\pi r_{cr}^2$, is approximately independent of the parameters a and b but *is* dependent on the luminosity and on the $(M/L)^*$ and r_e^* normalizations.

Figure 4 shows the effect on the lensing probabilities of the parameters described above, as reflected in the numerical calculation. In Figure 4*a*, we plot as a function of luminosity the product bias $r_{cr}^2 \times \phi_g(L)$ (i.e., the distribution of galaxies that lens), for various values of a. Note that the area under the curves (proportional to the total lensing probability due to galaxies at that redshift) is similar for the various curves. The stronger dependence of the lensing probability on $(M/L)^*$ and r_e^* is shown in Figures 4*b* and 4*c*.

6.1.2. *Predicted Lensing Frequencies and Separation Distributions*

Using the adopted values of all the parameters and integrating the lensing cross section over lens luminosity and redshift and over all 502 quasars in the snapshot sample, we obtain the predicted number of lensed quasars and their image separation distribution.

Figure 5 shows the expected distribution, $n(\theta)$, for early-type galaxies without halos for an empty ($\Omega = 0$) and for a flat ($\Omega = 1$) universe, superposed on the distribution of observed lenses. (This distribution, whose binning is somewhat arbitrary, is shown for illustrative purpose only; the statistical methods used for comparing between the models and the observations are described in Section 5.) Neither model provides a good fit to the observations. Virtually no lenses larger than 2″ are predicted, independent of cosmology. This can be quantified by drawing Monte Carlo observations (see § 5) from the predicted distributions and comparing the distribution of likelihoods to the observed likelihood: none of 5000 draws yield a likelihood as low as observed for either $\Omega = 0$ or $\Omega = 1$.

Table 1 lists the above two models and subsequent models, which we calculate below. For every model, we give the total number of predicted lenses, the relative likelihood defined by equation (64), and the Monte Carlo probability of the observed statistics, given the model.

© American Astronomical Society • Provided by the NASA Astrophysics Data System

1993ApJ...416..425M

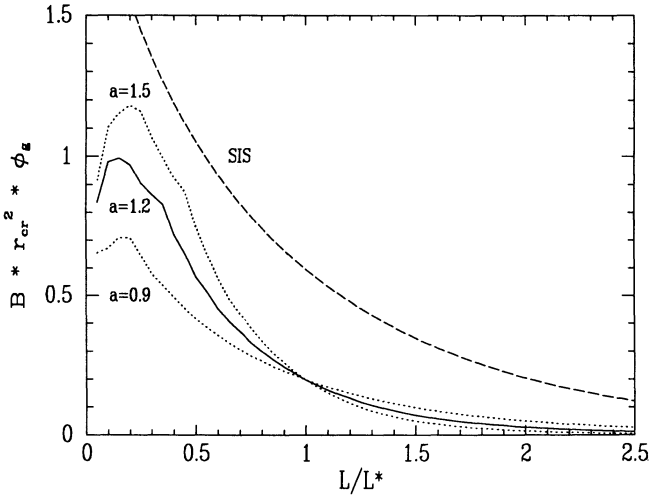

FIG. 4a

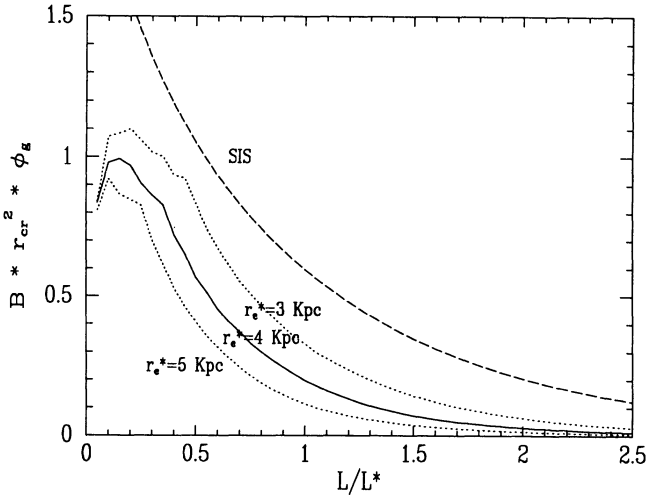

FIG. 4b

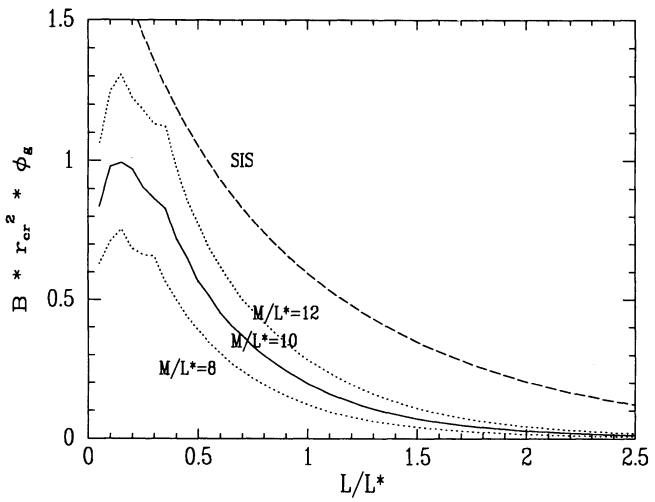

FIG. 4c

FIG. 4.—The luminosity distribution of lensing galaxies (i.e., the distribution of galaxy luminosities weighted by the lensing cross section at each luminosity), again for $z_{lens} = 0.5$, $z_{quasar} = 2.0$, and quasar $M_V = -25.5$. The dependence of this function on three of the model parameters is shown: (*a*) the power-law index a; (*b*) the effective radius r_e^* of an L^* galaxy; and (*c*) the mass-to-light ratio (M/L^*) of an L^* galaxy. The probability of lensing by galaxies at $z = 0.5$ is proportional to the areas under the curves.

There are two parameters which may be thought to increase significantly the chance of finding wider separation lenses: M/L and r_e. Both parameters can increase the mean mass surface density within a given radius. Can changes of these parameters within their uncertainties yield more satisfactory separation distributions? Figure 6*a* shows the effect of varying the mean M/L^* and Figure 6*b* the effect of varying r_e^*. Even though increasing M/L and decreasing r_e yields significantly better (in a relative likelihood sense) fits, they still predict only a very small probability of finding lenses with $\Delta\theta > 2''$. Quantitatively, only 0.5% of all Monte Carlo draws from $n(\theta)$ yield a probability as low as observed. A $(M/L)^*$ greater than 15, strongly inconsistent with kinematic observations of early-type galaxies, is required in order to reproduce the observed lensing statistics with at least 5% probability Changes in the other parameters, a, b, within their uncertainty limits have even less of an effect.

We conclude, independent of the exact choices of the structural parameters for the lenses, that the *predicted separation distribution does not match the observations if early-type galaxies have constant M/L ratios at all radii.*

6.2. *Lensing by Early-Type Galaxies with Halos*

For an initial discussion of the effect of halos, we keep all of the structural parameters of the luminous part of the lens fixed at their "standard" values and only discuss $\Omega = 1$ and $\Omega = 0$.

The halo parameter most important for the lensing statistics is the core radius, r_c; this sensitivity is illustrated in Figure 7*a*, which plots the distribution of separations for various values of r_c/r_e. In order for the halo to affect the lensing statistics, the halo core radius must be small enough ($r_c/r_e \sim 1$) to prevent the bending angle, $\alpha(r) \propto M(<r)/r$, from decreasing substantially outside of its maximum at $\sim 0.16 r_e$. Even though this effect of the halo on the bending angle leaves the lensing cross section virtually unchanged, it leads to a doubling of the expected number of lenses and to a dramatic increase in the probability of finding images with separations $\gtrsim 1''.5$. Lenses with a flat (rather than falling) bending angle curve produce larger image separations and stronger magnification biases. Figure 7*b* shows $n(\theta)$ for various σ^* at a given r_c/r_e. The last remaining dark halo parameter is a power-law index c which governs $\sigma(L)$. The dependence of $n(\theta)$ on c is relatively weak, and models between the limiting cases of $\sigma \propto L^{1/2}$ and

© American Astronomical Society • Provided by the NASA Astrophysics Data System

1993ApJ...416..425M

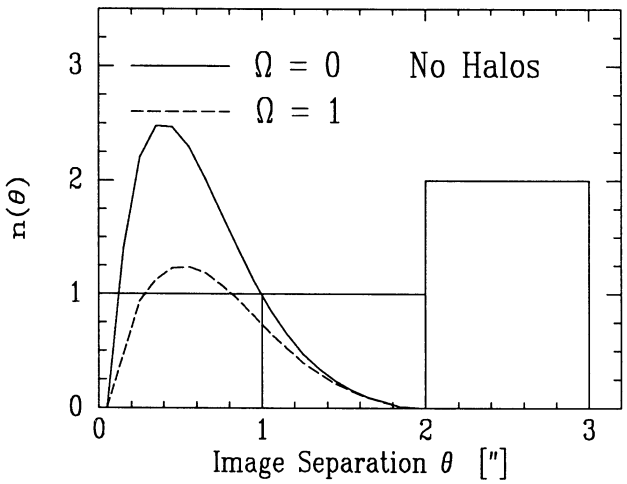

FIG. 5.—The expected distribution of observed lens image separations in flat and empty universes, if early-type galaxies are assumed to have a mass profile proportional to their light (i.e., no dark halos). Independent of cosmology, such a model predicts virtually no lenses with separations larger than 2″. The plotted rectangles indicate the image-separation distribution of the four lensed quasars in the snapshot survey. (This distribution, whose binning is somewhat arbitrary, is shown here and in the following figures for illustrative purpose only; the statistical methods used for comparing between the models and the observations are described in § 5.)

$\sigma \propto L^{1/4}$ (the Faber-Jackson relation) have similar likelihoods. As an example, for $\sigma^* = 250$ km s^{-1} and $r_c/r_e = 1$, the relative likelihoods for $\sigma \propto L^{1/2}$ and $\sigma \propto L^{1/4}$ differ by less than unity.

The Monte Carlo simulations (§ 4.2) show that, for the best models, the observed likelihood falls well within ($\sim$30 percentile) the distribution of likelihoods of pseudoobservations drawn from the model. Hence, the best methods are consistent with the data in an absolute sense. Figure 8 shows the $\sigma^* - r_c/r_e$ plane in parameter space at $c = 0.4$, with contours showing the model probabilities. We see that the acceptable range for the dark halos of early-type galaxies is $r_c \sim r_e$ and $\sigma^* \gtrsim 270$ km s^{-1}. Models with lower σ^* or higher r_c/r_e fare significantly worse.

TABLE 1

MODELS AND PROBABILITIES

Model[a]	N[b]	L[c]	MC[d]
No halo, $\Omega = 1$	1.1	< -20	0.00
No halo, $\Omega = 0$	2.0	< -20	0.00
No halo, $M/L = 8, \Omega = 1$	0.8	< -20	0.00
No halo, $M/L = 12, \Omega = 1$	1.5	−7.8	0.08
No halo, $r_e^* = 5$ kpc, $\Omega = 1$	0.8	< -20	0.00
No halo, $r_e^* = 3$ kpc, $\Omega = 1$	1.5	−6.2	0.50
Halo $\sigma^* = 300$ km s^{-1}, $r_c/r_e = 4$	1.9	< -20	0.00
Halo $\sigma^* = 300$ km s^{-1}, $r_c/r_e = 2$	2.5	−7.6	0.22
Halo $\sigma^* = 300$ km s^{-1}, $r_c/r_e = 1$	3.5	−2.5	36.6[e]
Halo $r_c/r_e = 1$, $\sigma^* = 150$ km s^{-1}	1.5	< -20	0.00
Halo $r_c/r_e = 1$, $\sigma^* = 200$ km s^{-1}	1.9	−13.1	0.00
Halo $r_c/r_e = 1$, $\sigma^* = 250$ km s^{-1}	2.6	−4.1	2.60
No halo, $\Omega + \lambda = 1, \lambda = 0.7$	2.9	< -20	0.00
No halo, $\Omega + \lambda = 1, \lambda = 0.8$	3.7	< -20	0.00
No halo, $\Omega + \lambda = 1, \lambda = 0.9$	5.5	< -20	0.00
Halo, $\Omega = 0, \lambda = 0$	6.5	−3.4	10.6[e]
Halo, $\Omega + \lambda = 1, \lambda = 0.6$	8.3	−3.9	5.7[e]
Halo, $\Omega + \lambda = 1, \lambda = 0.7$	10.5	−5.2	1.60
Halo, $\Omega + \lambda = 1, \lambda = 0.8$	14.2	−7.7	0.08
Halo, $\Omega + \lambda = 1, \lambda = 0.9$	21.7	−13.5	0.00
No halo, bivar. (r_e, L) dist., $\Omega = 1$	2.4	−5.9	0.98
No halo, all in Coma cluster, $\Omega = 1$	2.8	−5.5	1.70
No halo, all in A370 cluster, $\Omega = 1$	3.2	−4.7	3.82
No halo, "error conspiracy"	8.2	−4.6	5.0[e]

[a] Short characterization of the model parameters. All parameters not listed are at their "standard" values, as listed in the text.

[b] Expected total number of lenses.

[c] Relative likelihood as defined in eq. (64).

[d] Absolute likelihood inferred from Monte Carlo simulations. The column entry gives the percentage of Monte Carlo draws from the model that yield a relative likelihood lower than that of the observed data.

[e] These models are statistically consistent with the data at a level greater than 5%.

© American Astronomical Society • Provided by the NASA Astrophysics Data System

1993ApJ...416..425M

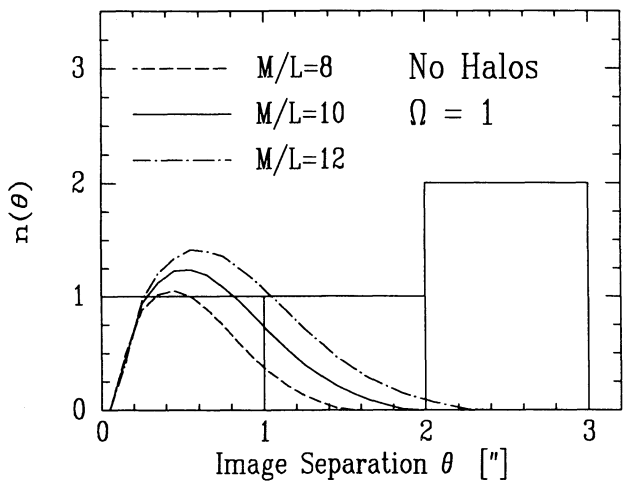

FIG. 6a

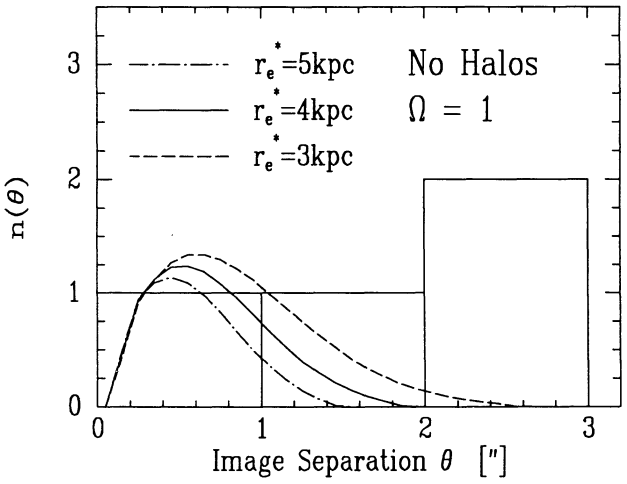

FIG. 6b

FIG. 6.—The distribution of image separations for the same model as in Fig. 5, but with the effect of uncertainties in some of the model parameters. (*a*) Variations in the mass-to-light ratio; (*b*) variations in the half-light radius of an L^* galaxy. Even with these uncertainties, there is a low probability of lensing above 2″ if galaxies do not have dark halos.

6.3. *Lensing and the Cosmological Constant*

The possibility that the universe has a nonzero cosmological constant λ has been recently revived (see Carroll, Press, & Turner 1992 for a review), mainly because of the "age problem," i.e., if H_0 is larger than 80 km s^{-1} Mpc^{-1}, then the age of the universe is in conflict with the estimated age of globular clusters, unless $\lambda > 0$. Moreover, if Ω_0 turns out to be less than unity, then one way to save the inflation model, which usually implies zero curvature, is to have nonzero λ, such that $\Omega_0 + \lambda = 1$. Gott, Park, & Lee (1989); Fukugita, Futamese, & Kasai (1990); F&T; and Kochanek (1992) have shown that lensing statistics can constrain λ. Bahcall et al. (1992a) and Maoz et al. (1992b, 1993a, b) followed F&T and used the SIS model to show that the total number of lenses observed in the snapshot survey is smaller then would be expected if $\lambda \gtrsim 0.8$. We investigate here whether this conclusion is valid for the more realistic galaxy models that we use in the present work and whether a cosmological constant can allow us to avoid the inference that early-type galaxies have dark halos. Using equations (57–61) to account for the geometrical effects of lensing in a flat universe with nonzero λ, we calculate the number distribution of image separations.

Figures 9*a* and *b* show the calculated distributions of galaxies with and without dark halos, for various values of λ. We see that, for a given galaxy model, the normalization of the distribution is sensitive to the cosmology, but the shape of the distribution is not. Models with large λ and no dark halos overpredict the number of small separation lenses. Models with large λ *and* galactic dark halos overpredict the total number of lens systems. We note that the predictions of $\Omega = 1$ and $\Omega = 0$ models are similar and cannot be discriminated by the observations.

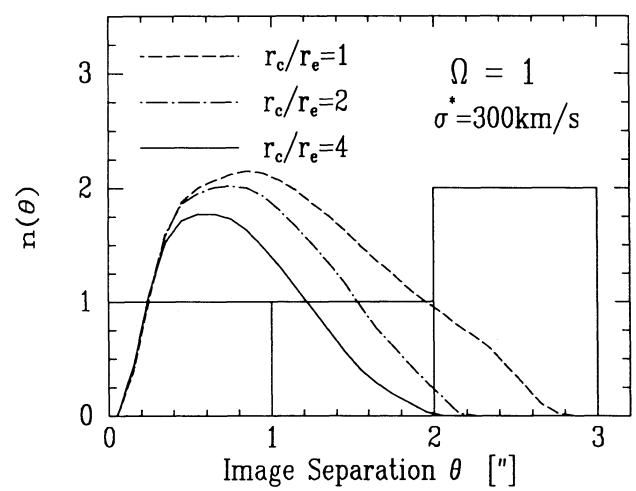

FIG. 7a

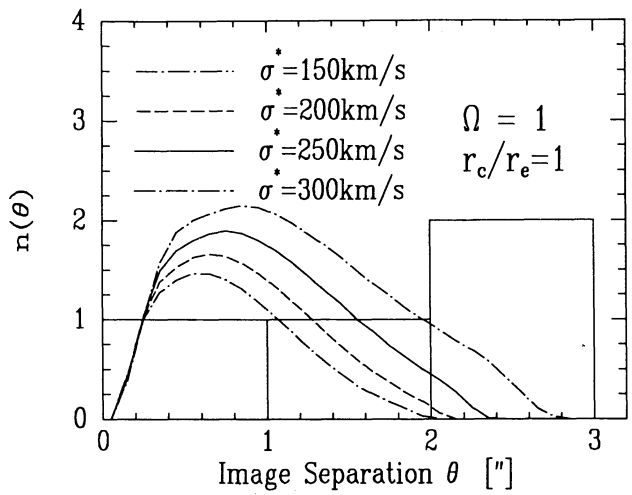

FIG. 7b

FIG. 7.—The distribution of image separations when galaxy mass profiles are modeled with the combination of a de Vaucouleurs profile proportional to the light (as in Fig. 5) *and* a dark isothermal halo. (*a*) The effect of varying the ratio of the dark halo core radius r_c to the half-light radius r_e. (*b*) The effect of varying the asymptotic velocity dispersion σ^* of the halo of an L^* galaxy. Both $r_c/r_e \sim 1$ and $\sigma^* > 250$ km s^{-1} are needed for the halo in order to predict a significant probability for lensing above 2″.

© American Astronomical Society • Provided by the NASA Astrophysics Data System

1993ApJ...416..425M

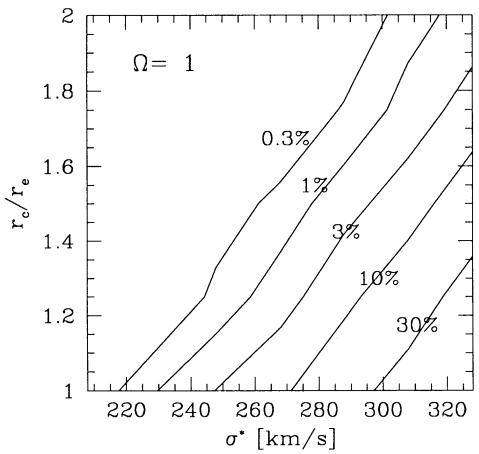

FIG. 8.—Parameter plane for two of the three parameters defining the dark halos of early-type galaxies: the line-of-sight asymptotic velocity dispersion σ^* and the ratio of core radius to effective radius. Contours indicate the probability of various parameter combinations, as determined by statistical comparison between the model and the observations (see § 5). Models with too small σ^* or too large r_c/r_e can be rejected. Similar limits are obtained for an $\Omega = 0$ universe.

Formally, all λ models can be rejected at least at the 99.5% level if the lenses have no halos. For galaxies with halos ($r_c/r_e = 1$, $\sigma^* = 300$ km s^{-1}), we can rule out values of $\lambda > 0.7$ at the 95% confidence level and $\lambda > 0.8$ at the 99.5% confidence level. Note that, for $\lambda < 0.7$ and $H_0 = 80$ km s^{-1} Mpc^{-1}, the age of the universe $t_0 < 0.96 \times H_0^{-1} = 12.2$ Gyr. Cosmologies with a cosmological constant are therefore no longer superior to low-density open cosmologies for solving the age problem.

In our calculations, we have implicitly assumed that the lensing galaxies are transparent. Present-day early-type galaxies appear to be quite transparent. For example, Bregman, Hogg, & Roberts (1992) estimate that an L^* elliptical galaxy contains about $10^5\ M_\odot$ of dust. If this mass of dust were evenly distributed within one effective radius and it had similar absorption properties to Galactic dust, objects passing through the galaxy would suffer only 0.1 mag of extinction, which would have little effect on lensing statistics.

If the same amount of dust were in optically thick clumps (as is normally the case in observed dusty galaxies), it would affect the lensing statistics even less, because only a fraction of the light paths through the galaxy would be blocked. Furthermore, Lauer (1988) finds that the isophotes in superposed cluster ellipticals are very regular after decompositions. If the dust had a radial profiles similar to that of the stars, Lauer's data also imply mean optical depths of only a few percent for the inner parts of ellipticals.

In an attempt to reconcile the small number of observed lensing events with a λ-dominated cosmology, Fukugita & Peebles (1993) have recently speculated that early-type galaxies may have been dustier, and therefore opaque, at redshifts $z \sim 0.5$–1. Although there is evidence that many disk galaxies have undergone star-formation since $z \sim 1$, producing dust in the process, several observational results point *against* such activity in massive ellipticals, which are the dominant lensing population. Bower, Lucey, & Ellis (1992) infer from the tight color-luminosity relation of elliptical galaxies in the Virgo and Coma clusters that the stars in these galaxies most likely formed at $z > 2$. Dunlop & Peacock (1993) find that the colors of 3CR gaxies at $z \sim 1$, when compared to

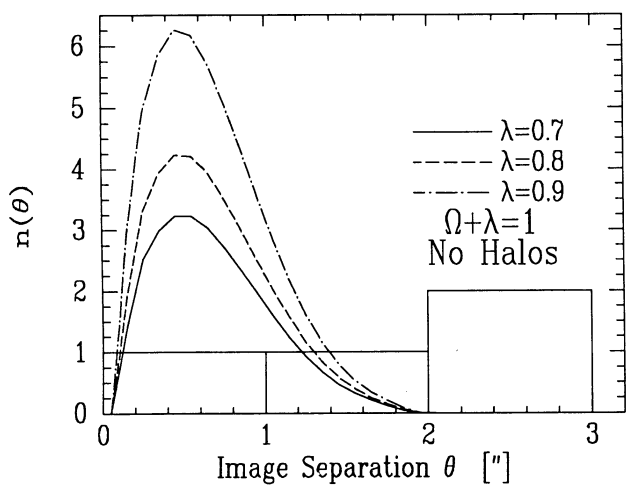

FIG. 9a

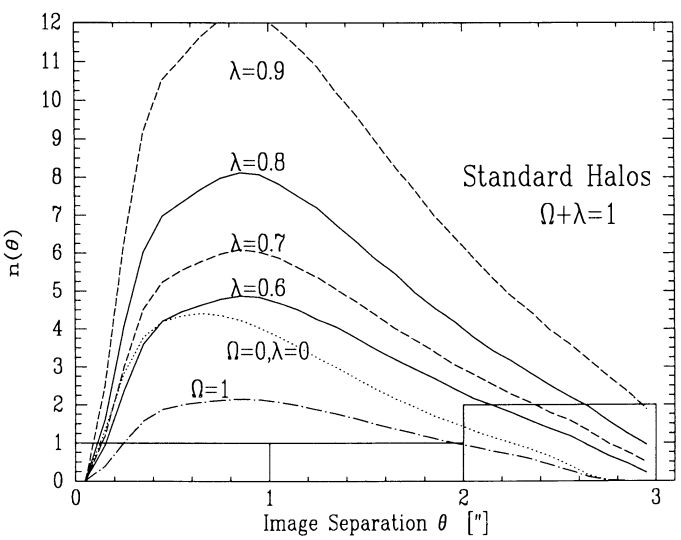

FIG. 9b

FIG. 9.—The effect of a cosmological constant λ on the distribution of image separations. (*a*) Models without dark halos; (*b*) models with isothermal dark halos, with $r_c/r_e = 1$, and $\sigma^* = 300$ km s^{-1}. Large-λ models are always a poor match to the observations.

© American Astronomical Society • Provided by the NASA Astrophysics Data System

1993ApJ...416..425M

present day ellipticals, indicate little star formation activity since $z \sim 1$. Dressler (1993) finds from analyzing an *HST* image of a $z \sim 0.4$ cluster that the blue galaxies producing the Butcher-Oemler effect are spiral and interacting galaxies, while the ellipticals in the cluster have the colors of present-day ellipticals. Therefore it seems that most ellipticals had their star-forming, and hence dusty, epoch at redshifts too large to affect lensing statistics.

6.4. *Other Effects*

6.4.1. *Lensing by Spiral Galaxies*

In our calculations thus far, we have considered only lensing by early-type (E and S0) galaxies. Previous calculations have shown that spiral galaxies, despite their overabundance relative to ellipticals and S0's, play a minor or negligible role in statistics lensing, because of their lower velocity dispersions. F&T found that in the SIS approximation, spirals contribute $\sim 17\%$ as much as ellipticals and S0's to the lensing probability. Hinshaw & Krauss (1987) assumed a constant isothermal core radius of 1 kpc for all spirals, and found that the lensing probability is only 6×10^{-5} as much as that of ellipticals.

In our calculations, we treat separately early (Sa–Sbc) and late (Sc–I) spiral types, since EEP find that the late types follow a Schechter luminosity function with a characteristic luminosity about 1 mag fainter than other galaxies. We assume that half of the spirals are early types and half are late types. For the early spiral types, if we assume that 0.6 of the total luminosity is in the bulge and that the core radius of the isothermal mass distribution $r_c = 0.16 r_e$ of the bulge, we find the contribution is only $\lesssim 2\%$ as much as that of the ellipticals + S0's to the lensing. Late spiral types have bulges that are considerably less concentrated than those of early-type spirals (Kent 1985). Under the assumption that the isothermal core radius is a fraction of the bulge effective radius, and considering the fact that their characteristic luminosity (and hence asymptotic velocity dispersion) is lower than that of early types, late spiral types are then even less important. Spiral galaxies therefore contribute $\lesssim 5\%$ to the lensing probability. The reduction in cross-section compared to the SIS calculation comes about because of the nonzero core size, which makes r_{cr} smaller or zero (i.e., makes some lenses subcritical). We conclude, in agreement with Hinshaw & Krauss (1987) and F&T, the spiral galaxies make only a small contribution to the lensing probability, a contribution that is insufficient to affect our conclusions.

6.4.2. *The Effect of a Bivariate Luminosity-Radius Distribution*

In the calculations described so far, we have assumed an exact correlation (the mean observed relation in eq. [7]) between galaxy effective radius and luminosity. In reality, there is a spread in the sizes of galaxies of a given luminosity. The bivariate distribution function of elliptical galaxies has been studied by several workers, notably Choloniewski (1985) and Sodré & Lahav (1993). They find that the bivariate distribution can be described as a Gaussian distribution about the linear relation between log R and log L. They find similar values for the Gaussian width, of 0.15 and 0.12 in log (R), respectively.

In order to study what effect the assumption of a monovariate distribution has on the lensing calculation, we have carried out the more general calculations for several parameter combinations. In these more realistic simulations, we have drawn log r_e from a Gaussian distribution in a Monte Carlo process. The Gaussian has a mean determined by equation (7) and a dispersion $\sigma = 0.15$. We find that use of the bivariate distribution to determine L and r_e slightly skews the distribution of angular separations to larger values, compared to the calculation using a monovariate function. Two percent of the lensed quasars are predicted to have separations greater than 2″. This effect, shown in Figure 10 and Table 1, comes about owing to the occasional appearance of galaxies with small effective radii, i.e., large surface brightness. Because of the stronger dependence of the angular distribution on r_e (see Fig. 6*b*), these deviations are not canceled by the large-r_e fluctuations. However, we see from Figure 10 that the overall effect is small and will therefore not affect our conclusions in the previous sections.

6.4.3. *The Effect of Clusters*

The surface-mass density of the clusters in which galaxies are often embedded can affect the observed lensing statistics. To investigate the magnitude of this effect and see whether it can change our conclusions regarding the existence of dark halos, we have made calculations that include clusters for some of the previous parameter combinations. In order to provide an upper limit to the effect of clusters, we have assumed in the calculation that all early-type galaxies have no dark halos but reside in galaxy clusters similar to the Coma cluster. This is an extreme assumption, since the fraction of early-type galaxies that are inside an Abell radius of a cluster of richness class $R \geq 0$ and the fraction of clusters that are as rich as Coma ($R = 2$) are each of order 10% (e.g., Bahcall 1993).

To carry out this calculation, we assign to each galaxy a location at a radius R_{cl} in the cluster. The location is drawn in a Monte Carlo fashion from an isothermal distribution of galaxies. The cluster has a core radius of $R_{core} = 0.15$ Mpc and a cutoff radius of 1.5 Mpc. The cluster surface mass density at R_{cl} (assumed to be constant on the scale of the galaxy) is

$$\Sigma_{cl} = \frac{\sigma_{cl}^2}{2G} (R_{cl}^2 + R_{core}^2)^{-0.5} , \tag{67}$$

where σ_{cl} is the asymptotic line-of-sight velocity dispersion of the cluster. In line with our extreme assumptions, we choose a velocity dispersion somewhat larger than is found for Coma (e.g., The & White 1986),

$$\sigma_{cl} = 1000 \text{ km s}^{-1} . \tag{68}$$

For these parameter values, $\Sigma_{cl} \sim 0.1$ g cm^{-2} in the core of the cluster. We then add a term $(\Sigma_{cl}/\Sigma_{cr})x_1$ to equation (33) and Σ_{cl}/Σ_{cr} to the left-hand side of equation (35) and proceed as before to calculate the lensing statistics.

Figure 11 shows the results of this calculation. A bivariate radius-luminosity distribution, as in the previous subsection, has been used. As expected (see, e.g., TOG), the addition of the cluster mass skews the distribution of image separations to larger values. The

© American Astronomical Society • Provided by the NASA Astrophysics Data System

1993ApJ...416..425M

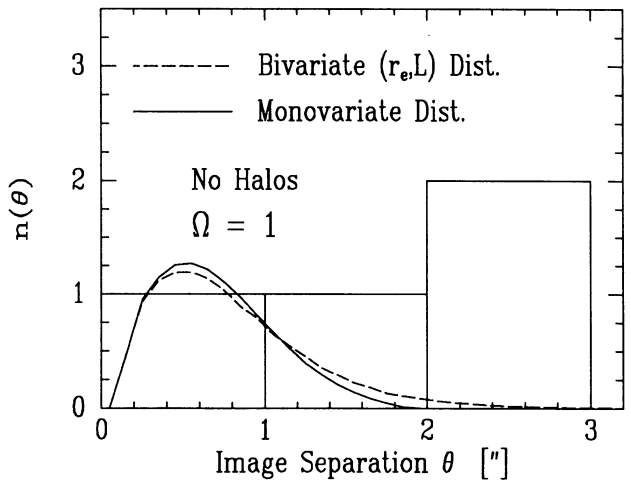

FIG. 10

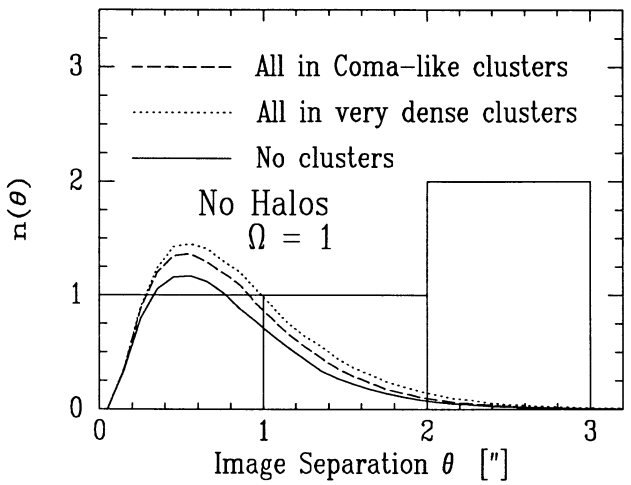

FIG. 11

FIG. 10.—The effect of using a bivariate effective-radius luminosity distribution function for the calculation, compared to use of the monovariate (Schechter) luminosity function, as in Fig. 5. The bivariate function has a small effect on the image distribution and does not change the conclusion that dark halos must be present in early-type galaxies.

FIG. 11.—The effect of placing all early-type galaxies in Coma-like clusters (*dashed curve*) or in dense Abell 370–like clusters (*dotted curve*). The relatively small addition of the central cluster surface mass density to that of some of the galaxies has little effect on the lensing statistics.

effect is, however, small, even under the extreme assumptions we have made concerning the role of clusters. Formally, this model can be rejected at the greater than 98% level. This should not come as a surprise, since only about 10% of the galaxies are in the core of the cluster, and even there, the cluster surface mass density constitutes only a 30% increment to the average surface mass density of an L^* galaxy.

Implicit in the model we have just described is the assumption that the dark matter distribution in clusters is smooth and follows the galaxy distribution. There is evidence that this is not always the case. Grossman & Narayan (1989) found that the dark matter in the cluster Abell 370 displaying gravitationally lensed arcs must be considerably more concentrated than the galaxy distribution, with a core radius of <80 kpc and $\sigma_{cl} \sim 1400$ km s^{-1} Tyson et al. (1993) have found that, in about 30% of rich and X-ray bright clusters, the geometrical alignment of background galaxies implies cluster dark matter core radii as small as ~ 50 kpc. Can these dense clusters assist haloless galaxies to form lens systems with separations of a few arcseconds?

We have repeated the previous calculation, in which every galaxy is in a cluster, with the core radius for the galaxy distribution of 150 kpc, but with a dark matter core radius of 50 kpc and velocity dispersion $\sigma_{cl} = 1400$ km s^{-1}. The dotted curve in Figure 11, resulting from this calculation, shows that even these extreme assumptions make little difference in the results. The reason is that such dense clusters can have supercritical surface density in their central regions and can therefore lens by themselves the background quasars. When a quasar is projected inside the critical lensing radius of the *cluster*, the resulting image separations (due to the potential with $\sigma \sim 1400$ km s^{-1} rather than ~ 300 km s^{-1}) will be of order arcminutes, rather than arcseconds. Thus, any galaxies within the cluster critical radius become ineffective for arcsecond-separation lensing.

The only way to create lenses with few arcsecond separation is with mass distributions having velocity dispersions of no more than several hundred km s^{-1}. Since the cross section for lensing is proportional to σ^4, these systems have to be abundant enough to explain the observed number of lensed quasars with such separations. The most natural place for these abundant dark matter concentrations is in the halos of early-type galaxies.

6.4.4. *The Effect of Uncertainties in the Model Parameters*

Although most of the parameters involved in our calculation have relatively well measured values (only the early-type galaxy dark halo characteristics and the cosmology have been treated as free parameters), we now examine the possibility that the combined uncertainties in several parameters may affect our conclusions. Figure 12 shows $n(\theta)$ calculated using the "best" values for all measured modeled parameters and assuming early-type have no dark halos and $\Omega = 1$. L and r_e are drawn from a bivariate distribution function, as in § 6.4.2. The dashed line in Figure 12 shows the effect of simultaneously shifting the values of all of the following parameters to their extreme values, each in the direction that will skew $n(\theta)$ to larger separations and higher normalization: $a = 1.5$, $r_e^* = 3$ kpc, $b = 0.35$, $(M/L)^* = 12$, and $M^*_{Q0} = -19.75$. Furthermore, every galaxy is in a Coma-like cluster. We see that, under such a conspiracy among the errors of many of the measured parameters, the number of large-separation lenses increases and the distribution is more similar to that resulting from some of the acceptable models with dark halos (see Fig. 7*b*). We conclude that under such an unlikely conspiracy among the errors in the parameters, the need for dark halos could perhaps be avoided. Improved measurements of the galaxy parameters, the quasar luminosity function, and the properties of clusters will reveal if this is a real possibility.

6.5. *Completeness of the Snapshot Survey*

Our calculations allow us to estimate the completeness of the snapshot survey. To do this, we calculate the lensing statistics for the most realistic model (i.e., with the standard parameter values, a dark halo of $\sigma^* = 300$ km s^{-1}, a bivariate luminosity-radius

© American Astronomical Society • Provided by the NASA Astrophysics Data System

1993ApJ...416..425M

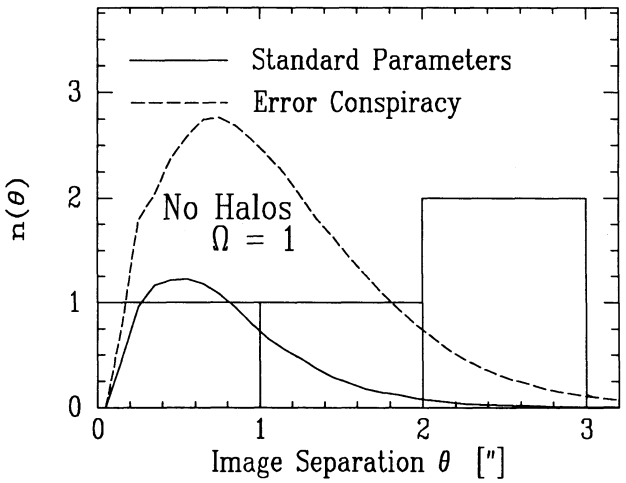

FIG. 12

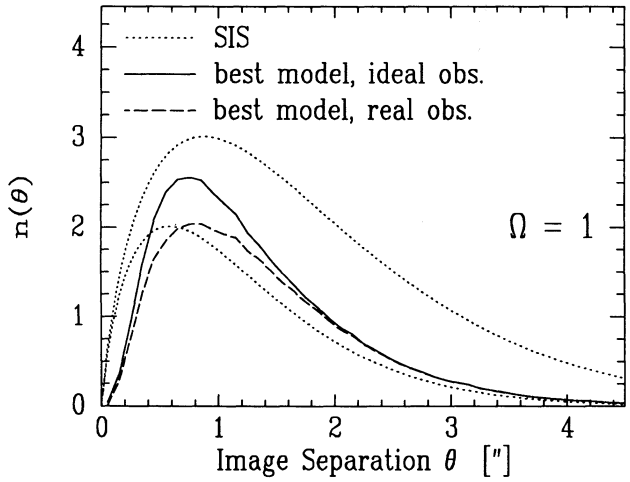

FIG. 13

FIG. 12.—The affect of combined uncertainties in the model parameters. The solid curve shows the angular separation distribution for a model in which early-type galaxies have no dark halos, 10% of the galaxies are in Coma-like clusters, and L and r_e of the galaxies are drawn from a bivariate distribution (see § 6.4.2 and Fig. 10). To create the dashed curve, five of the most important model parameters have been simultaneously offset by their uncertainties, all in the sense that will increase the number of predicted large-separation lenses. The offset parameters values are: $a = 1.5$, $b = 0.35$, $M/L^* = 12$, $r_e^* = 3$ kpc, $M_{Q0} = -19.75$. In addition, all galaxies are assumed to be in Coma-like clusters. Only under such an unlikely conspiracy of the errors do models without dark halos predict a significant number of large-separation lenses.

FIG. 13.—Snapshot survey completeness and comparison to the SIS approximation. The solid and dashed curves are the distributions predicted by a standard model with dark halos, before and after application of the snapshot survey detection limits. The two dotted curves give the predictions of the SIS approximation, with the $(3/2)^{1/2}$ factor applied to the observed stellar velocity dispersion (*upper dotted curve*) and without it (*lower dotted curve*).

distribution, and 10% of the galaxies in Coma-like clusters), but assuming a *perfect* detection function, i.e., in equation (37), $D = 1$ always. We thus obtain the intrinsic distribution from which the observed image-separation distribution is derived. The assumptions here are that the detection function (which was determined independently of the observations) has been correctly characterized and that the best model, combined with the detection function, can reproduce the observations. The two distributions are shown in Figure 13 as solid and dashed curves. We see that the snapshot survey is nearly complete (i.e., rarely classifies a lensed quasar as unlensed) at separations $\gtrsim 1\farcs5$. At separations $< 1\farcs5$ the survey is 85% complete. Since the survey has found only one subarcsecond lens, probably no lensed quasars were misclassified as unlensed because of the detection limits of the survey.

6.6. *Comparison with the SIS Approximation*

A final question we now address is: how accurate is the SIS approximation which has often been used in lensing statistics calculations? For this purpose, we compare the intrinsic and the detection-limited distributions calculated in the previous subsection to the distribution predicted by the SIS approximation. This is instructive because almost all previous lensing statistics work uses some form of the SIS model and because the simplicity of calculations with that model may still make it attractive in the future. The dotted curves in Figure 13 show the results of two versions of SIS, calculated using the formalism and parameters given by F&T. No observational biases are incorporated in the SIS curves, except for the magnification bias. The two SIS curves are obtained depending on whether or not the observed stellar velocity dispersions of early-type galaxies are scaled by a factor $(3/2)^{1/2}$ (see § 2.1). There has been some debate at to whether the $(3/2)^{1/2}$ factor should be applied.

We see in Figure 13 that our best "intrinsic" model (*solid curve*) is bracketed by the two SIS models. Interestingly, the distributions from the "detected" model (*dashed curve*) for the snapshot survey and from the SIS approximation *without* the $(3/2)^{1/2}$ factor are very similar in terms of both their shape and total number of lenses. Although the details of the mass distribution in galaxies is considerably more complicated than assumed in the SIS model, the final distribution of image separations that SIS predicts is basically correct and is consistent with the observed lensing statistics.

7. SUMMARY AND CONCLUSIONS

The *HST* snapshot survey provides a useful statistical database for comparing the theory and the observations of gravitational lensing. We have compared the survey results, for separations greater than $0\farcs1$, to the predictions of the frequency and angular separation distribution of parameterized models for the lenses and for the background cosmology. In particular, we have investigated whether the data favor massive dark halos in early-type galaxies, the main lensing population, over constant M/L models and what limit can be set on the values of the cosmological constant in flat cosmologies.

We obtain results of high statistical significance even though the number of observed lens systems in the survey that may be due to individual galaxies is small (four). The statistical power of the conclusions arises partly because many models *underpredict* the number of lenses at large separations. In this respect our analysis is robust to the presence of possible selection biases (Kochanek 1991b). Our main results can be summarized as follows:

1. If most early-type galaxies had no dark halos, the models predict virtually all lenses to be at separations smaller than 2″. This hypothesis can be ruled out at the greater than 99.5% confidence level for otherwise standard galaxy parameters.

© American Astronomical Society • Provided by the NASA Astrophysics Data System

1993ApJ...416..425M

2. The observed and predicted angular distributions of multiple images are consistent if early-type galaxies generically have massive halos. The halos must have core radii small enough to "conspire" with the luminous matter to yield a flat rotation curve for $0.2r_e \lesssim r_c \lesssim 2r_e$. The inclusion of halos yields a much better match to the observations not because of an increase is the lensing cross sections, but because of an increase of the magnification bias and of the expected image splitting at a given luminosity. Despite the small number of observed systems, the inclusion of halos provides a statistically significant improvement over the models without halos. This result is insensitive to the assumed cosmology, since different cosmologies predict distributions of separations with similar shapes but with different normalizations.

3. If the universe is flat, the dimensionless cosmological constant $\lambda < 0.7$ at the 95% confidence level. This limit, which is derived by taking into account the angular separation distribution of lenses, is stronger than the upper limits that can be derived for λ based on the total number of lenses alone. Such values of λ imply an age for the universe similar to that of standard low-density cosmologies and are therefore not useful in terms of solving the "age problem" of the universe.

4. The effect of the host clusters of galaxies on the lensing statistics is small and cannot be used to avoid the need for dark halos in order to match the observations. This is true even if the host clusters are very dense. Only a small fraction of the galaxies are located in a part of the cluster that has the surface density required to enhance significantly the image separations produced by the galaxies alone.

5. Comparison of the intrinsic number of lensed quasars predicted by acceptable models to the number that would be identified under the detection limits of the snapshot survey shows that the survey is probably complete, i.e., no lensed quasars have been missed due to the detection limits.

6. All of the above conclusions are robust with respect to the observational uncertainties in the galaxy lens parameters.

We thank Andy Gould for numerous helpful discussions and comments in the course of this work. We have also greatly benefitted from valuable advice from John Bahcall, Neta Bahcall, George Djorgovski, Marijn Franx, Chris Kochanek, Ofer Lahav, Ramesh Narayan, Massimo Persic, Penny Sackett, Laerte Sodré, Ed Turner, Tony Tyson, and Brian Yanny. This work was supported by grant GO-2775 (D.M.) and a Hubble Fellowship HF-1025.01-91A (H.-W. R.) from the Space Telescope Science Institute, which is operated by the Association of Universities for Research in Astronomy, Inc., under NASA contract NAS5-26555.

REFERENCES

Ashman, K. M. 1992, PASP, 104, 1109
Bacon, R. 1985, A&A, 143, 94
Bahcall, J. N., & Casertano, S. 1985, ApJ, 293, L7
Bahcall, J. N., Hartig, G., Jannuzi, B. T., Maoz, D., & Schneider, D. P. 1992c, ApJ, 400, L51
Bahcall, J. N., Maoz, D., Doxsey, R., Schneider, D. P., Bahcall, N. A., Lahav, O., & Yanny, B. 1992a, ApJ, 387, 56
Bahcall, J. N., Maoz, D., Schneider, D. P., Yanny, B., & Doxsey, R. 1992b, ApJ, 392, L1
Bahcall, N. A. 1993, in Astrophysical Quantities, ed. C. W. Allen, in press
Barnes, J. 1987, in Nearly Normal Galaxies, ed. S. Faber (New York: Springer), 154
Bernstein, G., Tyson, A., & Kochanek, C. S. 1993, AJ, 105, 816
Blandford, R. D., & Kochanek, C. S. 1987, ApJ, 321, 658
Blandford, R. D., & Narayan, R. 1992, ARA&A, 30, 311
Bower, R. G., Lucey, J. R., & Ellis, R. S. 1992, MNRAS, 254, 601
Boyle, B. J., Fong, R., Shanks, T., & Peterson, B. A. 1987, MNRAS, 227, 717
Blumenthal G., Faber S., Flores R., & Primack J. 1986, ApJ, 301, 27
Bregman, J. N., Hogg, D. E., & Roberts, M. S. 1992, ApJ, 387, 484
Broeils, A. 1992, Ph.D. thesis, Univ. of Groningen
Caroll, S. M., Press W. H., & Turner, E. L. 1992, ARA&A, 30, 499
Casertano, S., & van Gorkom, J. H. 1991, AJ, 101, 1231
Choloniewski, J. 1985, MNRAS, 214, 197
de Carvalho, R. R., & da Costa, L. N. 1988, ApJS, 68, 173
de Vaucouleurs, G. 1948, Ann. d'Astrophys., 11, 247
de Zeeuw, P. T., & Franx, M. 1991, ARA&A, 29, 239
Dressler, A. 1993, Proc. of Milan Conf. on Observational Cosmology, in press
Dunlop, J. S., & Peacock, J. A. 1993, MNRAS, in press
Dyer, C. 1984, ApJ, 287, 26
Efstathiou, G., Ellis, R. S., & Peterson, B. A. 1988, MNRAS, 232, 431 (EEP)
Faber, S. M., Dressler, A., Davies, R. L., Burstein, D., Lynden-Bell, D., Terlevich, R., & Wegner, G. 1987, in Nearly Normal Galaxies, ed. S. M. Faber (New York: Springer), 175
Franx, M. 1993, in IAU Symp. 153, Galactic Bulges, ed. H. De Jonghe & H. Habing (Dordrecht: Reidel), in press
Freedman, W. L. 1990, ApJ, 355, L35
Fukugita, M., Futamese, T., & Kasai, M. 1990, MNRAS, 246, 25p
Fukugita, M., & Peebles, P. J. E. 1993, ApJ, submitted
Fukugita, M., Okamura, S., Tarusawa, K., Rood, H. J., & Williams, B. A. 1991, ApJ, 376, 8
Fukugita, M., & Turner, E. L. 1991, MNRAS, 253, 99 (F&T)
Goldschmidt, P., & Miller, L. 1991, in ASP Conf. Series, Vol. 21, The Space Distribution of Quasars, ed. D. Crampton (San Francisco: ASP), 212
Gott, J. R. 1977, ARA&A, 15, 239
Gott, J. R., Park, M. G., & Lee, H. M. 1989, ApJ, 338, 1
Grossman, S., & Narayan, R. 1989, ApJ, 344, 637
Gunn, J., Stryker, L., & Tinsley, B. 1981, ApJ, 249, 48
Hinshaw, G., & Krauss, L. M. 1987, ApJ, 320, 468
Jorgensen, I., Franx, M., & Kjaergaard, P. 1992, A&AS, in press
Kent, S. 1985, ApJS, 59, 115
———. 1990, in ASP Conf. Series, Evolution of the Universe of Galaxies, ed. R. G. Kron (San Francisco: ASP), 109
Kochanek, C. S. 1991a, ApJ, 373, 354
———. 1991b, ApJ, 379, 517
———. 1992, ApJ, 384, 1
———. 1993, ApJ, in press
Kochanek, C. S., & Blandford, R. D. 1987, ApJ, 321, 676
Kormendy, J. 1990, in ASP Conf. Series, Vol. 10 Evolution of the Universe of Galaxies, ed. R. G. Kron (San Francisco: ASP), 33
Kormendy, J., & Djorgovski, S. 1989, ARA&A, 27, 235
Kovner, I. 1987, ApJ, 321, 686
Krauss, L. M., & White, M. 1992, ApJ, 397, 357
Lauer, T. 1988, ApJ, 325, 49
Magain, P., Surdej, J., Vanderriest, C., Pirenne, B., & Hutsemekers, D. 1992, A&A, 253, L13
Majewski, S. R., Munn, J. A., Kron, R. G., Bershady, M. A., & Metanka, J. J. 1991, in ASP Conf. Series, Vol. 21, The Space Distribution of Quasars, ed. D. Crampton (San Francisco: ASP), p. 55
Mao, S. 1991, ApJ, 380, 9
Maoz, D., et al. 1992a, ApJ, 386, L1
Maoz, D., Bahcall, J. N., Schneider, D. P., Doxsey, R., Bahcall, N. A., Lahav, O., & Yanny, B. 1992b, ApJ, 394, 51
Maoz, D., et al. 1993a, ApJ, 409, 28
Maoz, D., Bahcall, J. N., Schneider, D. P., Doxsey, R., Bahcall, N. A., Lahav, O., & Yanny, B. 1993b, ApJ, 402, 69
Peletier, R. 1989, Ph.D. thesis, Univ. of Groningen
Persic, M., & Salucci, P. 1991, ApJ, 368, 60
Postman, M., & Geller, M. J. 1984, ApJ, 281, 95
Press, W. H., & Gunn, J. E. 1973, ApJ, 185, 397
Refsdal, S. 1964, MNRAS, 128, 295
Rix, H.-W. 1991, Ph.D. thesis, Univ. of Arizona, Univ. of Michigan Press
Rix, H.-W., Schneider, D. P., & Bahcall, J. N. 1992, AJ, 104, 959
Rubin, V., Burstein, D., Ford, W. K., & Thonnard, N. 1985, ApJ, 289, 81
Schweitzer, F., van Gorkom, J. H., & Seitzer, P. 1989, ApJ, 338, 770
Simien, F., & de Vaucouleurs, G. 1986, ApJ, 302, 564
Sodré, L., & Lahav, O. 1993, MNRAS, 260, 285
The, L. S., & White, S. D. M. 1986, AJ, 92, 1248
Turner, E. L. 1980, ApJ, 242, L135
———. 1990, ApJ, 365, L43
Turner, E. L., Ostriker, J. P., & Gott, J. R. 1984, ApJ, 284, 1 (TOG)
Tyson, A., et al. 1993, in preparation
Van der Marel, R. 1991, MNRAS, 253, 710
Wallington, S., & Narayan, R. 1993, ApJ, 403, 517
Weinberg, S. 1972, Gravitation and Cosmology (New York: Wiley)
Young, P., Gunn, J. E., Kristian, J., Oke, J. B., & Westphal, J. A. 1981, ApJ, 244, 736

© American Astronomical Society • Provided by the NASA Astrophysics Data System